Bioactive Materials 47 (2025) 1–17

Contents lists available at ScienceDirect

Bioactive Materials

journal homepage: www.keaipublishing.com/en/journals/bioactive-materials

Dermal fibroblast-derived extracellular matrix (ECM) synergizes with keratinocytes in promoting re-epithelization and scarless healing of skin wounds: Towards optimized skin tissue engineering

Xiangyu Dong [a], Han Xiang [a], Jiajia Li [a], Ailing Hao [a], Hao Wang [a,b], Yannian Gou [a], Aohua Li [a], Saidur Rahaman [a], Yiheng Qiu [a], Jiahao Li [a], Ou Mei [b,c], Jiamin Zhong [a,b], Wulin You [b,d], Guowei Shen [b,e], Xingye Wu [b,f], Jingjing Li [b,g], Yi Shu [b,h], Lewis L. Shi [b], Yi Zhu [b], Russell R. Reid [b,i], Tong-Chuan He [b,i,*], Jiaming Fan [a,j,**]

[a] *Ministry of Education Key Laboratory of Diagnostic Medicine, and Department of Clinical Biochemistry, School of Clinical Laboratory Medicine, Chongqing Medical University, Chongqing, 400016, China*
[b] *Molecular Oncology Laboratory, Department of Orthopaedic Surgery and Rehabilitation Medicine, The University of Chicago Medical Center, Chicago, IL, 60637, USA*
[c] *Department of Orthopedic Surgery, Jiangxi Hospital of Traditional Chinese Medicine, Jiangxi University of Traditional Chinese Medicine, Nanchang, 330006, China*
[d] *Department of Orthopaedic Surgery, Wuxi Hospital Affiliated to Nanjing University of Chinese Medicine, Wuxi, 214071, China*
[e] *Department of Orthopaedic Surgery, BenQ Medical Center, The Affiliated BenQ Hospital of Nanjing Medical University, Nanjing, 210019, China*
[f] *Department of Gastrointestinal Surgery, the First Affiliated Hospital of Chongqing Medical University, Chongqing, 400016, China*
[g] *Department of Oncology, The Affiliated Hospital of Shandong Second Medical University, Weifang, 261053, China*
[h] *Stem Cell Biology and Therapy Laboratory of the Pediatric Research Institute, the National Clinical Research Center for Child Health and Disorders, and Ministry of Education Key Laboratory of Child Development and Disorders, the Children's Hospital of Chongqing Medical University, Chongqing, 400016, China*
[i] *Laboratory of Craniofacial Biology and Development, Section of Plastic and Reconstructive Surgery, Department of Surgery, The University of Chicago Medical Center, Chicago, IL, 60637, USA*
[j] *Western Institute of Digital-Intelligent Medicine, Chongqing, 401329, China*

ARTICLE INFO

Keywords:
Dermal fibroblasts
Reversible immortalization
Extracellular matrix
Keratinocytes
Scarless wound healing
Skin tissue engineering

ABSTRACT

Skin serves as the first-order protective barrier against the environment and any significant disruptions in skin integrity must be promptly restored. Despite significant advances in therapeutic strategies, effective management of large chronic skin wounds remains a clinical challenge. Dermal fibroblasts are the primary cell type responsible for remodeling the extracellular matrix (ECM) in wound healing. Here, we investigated whether ECM derived from exogenous fibroblasts, in combination with keratinocytes, promoted scarless cutaneous wound healing. To overcome the limited lifespan of primary dermal fibroblasts, we established reversibly immortalized mouse dermal fibroblasts (imDFs), which were non-tumorigenic, expressed dermal fibroblast markers, and were responsive to TGF-β1 stimulation. The decellularized ECM prepared from both imDFs and primary dermal fibroblasts shared similar expression profiles of extracellular matrix proteins and promoted the proliferation of keratinocyte (iKera) cells. The imDFs-derived ECM solicited no local immune response. While the ECM and to a lesser extent imDFs enhanced skin wound healing with excessive fibrosis, a combination of imDFs-derived ECM and iKera cells effectively promoted the re-epithelization and scarless healing of full-thickness skin wounds. These findings strongly suggest that dermal fibroblast-derived ECM, not fibroblasts themselves, may synergize with keratinocytes in regulating scarless healing and re-epithelialization of skin wounds. Given its low immunogenic nature, imDFs-derived ECM should be a valuable resource of skin-specific biomaterial for wound healing and skin tissue engineering.

* Corresponding author. Molecular Oncology Laboratory, The University of Chicago Medical Center, Chicago, IL, 60637, USA
** Corresponding author. Ministry of Education Key Laboratory of Diagnostic Medicine, Department of Clinical Biochemistry, School of Clinical Laboratory Medicine, Chongqing Medical University, Chongqing, 400016, China.
E-mail addresses: tche@uchicago.edu (T.-C. He), fanjiaming1988@cqmu.edu.cn (J. Fan).

https://doi.org/10.1016/j.bioactmat.2024.12.030
Received 20 September 2024; Received in revised form 24 December 2024; Accepted 27 December 2024
Available online 8 January 2025

1. Introduction

As one of the most vital and largest organs in humans, the skin serves as a first-order protective barrier against the environment, and plays a role in immunologic surveillance, control of insensible fluid loss, sensory perception, and overall homeostasis. The skin typically consists of three layers, the epidermis (the outermost layer), the dermis (the layer below the epidermis); and hypodermis is the dermis, and the third and deepest layer is the subcutaneous tissue [1–3]. The epidermis has varied thicknesses in different types of skin and contains five sublayers with numerous cell types, notably keratinocytes and Langerhans cells (both in the squamous cell layer), and melanocytes (in the basal cell layer). Keratinocytes produce keratin, a tough and protective protein that is the major structural component of the skin, hair, and nails. The dermis is the thickest of the three layers, and contains dermal fibroblasts, hair follicles, sweat glands, sebaceous glands, blood vessels, lymph vessels, nerve endings, collagen and elastin. Dermal fibroblasts (Fibs) are the major cell population of the skin dermis and responsible for depositing and remodeling the extracellular matrix (ECM), as well as regulating tissue immunity, wound healing, and hair follicle development [4].

Skin integrity can be disrupted by trauma, surgery, and other chemical and pathological insults, and must be promptly restored in order to maintain its critical function. The repair of cutaneous wound requires the coordinated participation of multiple cell types and growth factors including peripheral blood mononuclear cells, resident skin cells, extracellular matrix, cytokines, chemokines, and numerous regulatory molecules [3,4]. Four overlapping phases are at play in the healing process: hemostasis, inflammation, proliferation, and remodeling. Of these phases, inflammation, proliferation, and remodeling determine whether the wound heals normally or aberrantly with excessive scar formation such as hypertrophic scars and keloids [1–3]. Dermal fibroblasts are the primary cell type responsible for remodeling the extracellular matrix (ECM) in wound healing by replacing the initial fibrin clot with hyaluronic acid, fibronectin, and proteoglycans, and later mature collagen fibers [1,3,5–7].

The ECM is the major component of the dermal skin layer and considered critical to wound healing and dermal regeneration. As a complex, heterogeneous network of soluble and insoluble molecules, dermal ECM provides a physical structural support to cell adhesion, proliferation, and differentiation [8]. It also provides a biochemical environment for cells to interact with biochemical components in the ECM such as integrins that are essential for epidermal maintenance through integrin-mediated anchoring of basal epidermal stem cells to the lower dermis through ECM proteins [9]. Furthermore, dermal ECM acts as a reservoir for growth factors, such as FGFs, VEGF, regulating their bioavailability via their binding to heparin and heparan sulfate, which are components of many ECM proteoglycans [10–12]. Adipose-derived mesenchymal stem cell-derived exosomes, which potentiated ECM hydrogels, accelerated diabetic wound healing and skin regeneration [13]. ECM-mimetic immunomodulatory hydrogels have been developed for the treatment of chronic skin wounds infected with methicillin-resistant *Staphylococcus aureus* [14]. In fact, ECM prepared from iPSC human lung fibroblasts have been shown to create a favorable microenvironment for wound repair, thereby enhancing wound healing [15,16]. The preparation of ECM often comes from primary cells, but the source of primary cells is scarce. Currently, the use of immortalized cell lines in human experiments is prohibited, but their derivatives—such as extracellular matrix and extracellular vesicles—are permitted for clinical applications. This underscores the necessity of developing immortalized dermal fibroblasts.

The intercellular crosstalk between epidermal keratinocytes and dermal fibroblasts is critical for skin homeostasis and wound healing [17,18]. Wound healing aims to restore the barrier function, which is accomplished by epithelial wound closure of the granulation connective tissue. We have recently demonstrated that exogenous keratinocytes facilitated re-epithelization and skin wound healing [19]. Mounting evidence suggests that well-coordinated interactions among dermal fibroblasts, keratinocytes, and dermal ECM may play an essential role in normal wound healing and skin regeneration.

In this study, we investigated the effects of interactions between dermal fibroblasts (Fibs) or ECM derived from dermal Fibs and keratinocytes on the scarless healing of cutaneous wounds. To overcome the limited lifespan of primary dermal fibroblasts, we established a reversibly immortalized mouse dermal fibroblast line (imDFs) by stably expressing SV40 large T antigen (SV40 T), which can be reversed by FLP recombinase. The imDFs are non-tumorigenic, express dermal fibroblast markers and are responsive to TGF-β1 stimulation. The ECM prepared from both imDFs (imDFs-ECM) and primary dermal Fibs (Fibs-ECM) shared similar expression profiles of extracellular matrix proteins, and promoted the cell proliferation of the previously immortalized mouse keratinocytes (iKera cells) [19]. The imDFs-derived ECM did not solicit significant local immune response. When delivered with the GelMa hydrogel, the ECM and to a lesser extent imDFs, effectively promoted mouse skin wound healing with excessive fibrosis. However, a combination of imDFs-derived ECM and iKera, delivered by GelMa hydrogel, effectively promoted the re-epithelization and scarless healing of wounds in a mouse model. These findings strongly suggest that dermal fibroblast-derived ECM, not fibroblasts themselves, may synergize with keratinocytes in controlling scarless re-epithelialization of wounds. Given its low immunogenic nature, imDFs-derived ECM should be a valuable resource of skin-related biomaterial for wound healing and skin regeneration.

2. Materials and methods

2.1. Cell culture and chemicals

HEK293 cells were obtained from American Type Culture Collection (ATCC, Manassas, USA). The immortalized mouse keratinocytes (iKera) and HEK-293 derivative 293pTP, RAPA, and 293 GP cells were previously described [19–22]. All cells were cultured in DMEM supplemented with 10 % fetal bovine serum (WISENT, Cat: 086–150, Australian) and 100 units of penicillin and 100 μg/mL of streptomycin in 5 % CO_2 incubators at 37 °C as previously described [23,24]. Unless otherwise specified, all chemicals were purchased from Solarbio (Beijing, China), Thermo Fisher Scientific (Waltham, MA, USA), or Sigma-Aldrich (St Louis, MO, USA).

2.2. Isolation of mouse dermal fibroblasts (Fibs)

The use and care of experimental animals were approved by the Research Ethics and Regulatory Committee of Chongqing Medical University, China, and the Institutional Animal Care and Use Committee of The University of Chicago. Mouse dermal fibroblasts (Fibs) were isolated from the skin tissue of newborn CD1 mice as described [19]. Briefly, newborn CD1 mice were euthanized, washed with sterile PBS, and sterilized with 70 % ethanol. The back skin was cut along the dorsal midline, loosened, and pulled to the ventral side. The full thickness skin was minced into 0.5–1.0 mm^3 pieces, directly seeded onto 100 mm cell culture dishes, and cultured at 37 °C in 5 % CO_2 in high glucose complete DMEM supplied with 10 % FBS. The medium was changed every 24 h to remove non-adherent cells. The adherent cells were passaged once reaching subconfluence (designated as P0, 1, 2, and 3, etc. to reflect the numbers of passages) for *in vitro* assays.

2.3. Establishment of the reversibly immortalized dermal fibroblasts (imDFs)

The isolated mouse dermal fibroblasts (less than 3 passages) were used to generate the immortalized dermal fibroblasts (imDFs). Briefly, the retroviral vector SSR#41, which expresses SV40 large T antigen (SV40 T) flanked with FRT sites [25,26], was co-transfected with the

pCL-Ampho packaging vector into HEK-293 cells to package SSR#41 retrovirus as described [27–29]. Subconfluent mouse dermal fibroblasts were infected with the packaged SSR#41 retrovirus. The infected dermal fibroblasts were treated with hygromycin B (0.3 mg/mL, Invitrogen) for 7–10 days, and then replated every 3 days. The resulting immortalized dermal fibroblasts were designated as imDFs and have been passaged for more than 30 generations.

2.4. Construction and amplification of recombinant adenoviral vectors Ad-FLP, Ad-TGFβ1, Ad-GFP and Ad-RFP

The AdEasy technology was used to generate recombinant adenovirus as described [30–32]. The construction and amplification of Ad-FLP and Ad-TGFβ1 were previously described [27,33]. Both Ad-GFP and Ad-RFP were used as controls as described [34]. Ad-FLP also expresses GFP, while Ad-TGFβ1 co-expresses RFP. All recombinant adenoviruses were packaged and/or amplified in 293pTP, RAPA, or 293 GP cells as described [20–22]. Fluorescence signals were captured using a fluorescence microscope. For all adenoviral infections, polybrene (8 μg/mL) was added to enhance infection efficiency as reported [30,35].

2.5. Immunofluorescence (IF) staining

The IF staining was performed as described [36,37]. Briefly, cells seeded on coverslips were fixed with 4 % paraformaldehyde for 30 min at room temperature (RT), treated with 0.5 % Triton X-100 for 10 min, and blocked with 5 % bovine serum albumin (BSA) for 30 min at RT. Primary antibodies (Table S2) were diluted in PBS and incubated on coverslips overnight at 4 °C. The secondary antibodies were incubated for 2 h at RT. Cell nuclei were counterstained with DAPI (10 μg/mL) for 10 min at RT. Fluorescent images were captured using a laser confocal microscope (Leica TCS SP8). Each assay condition was performed in triplicate.

2.6. Crystal violet cell viability assay

Crystal violet staining was conducted as described [38]. Briefly, exponentially growing cells were seeded in 24-well plates at a density of 10,000 cells per well. At the indicated timepoints, cells were gently washed with PBS and then stained with a 0.5 % crystal violet/formalin solution for 10 min. The plates were washed with tap water and air-dried before scanning. For quantitative analysis, the stained cells were dissolved in 10 % acetic acid and their absorbance at 592 nm was measured as described [19,39].

2.7. WST-1 cell proliferation assay

Exponentially growing cells were seeded in 96-well plates at a density of 3000 cells per well. At the indicated timepoints, the Premixed WST-1 Reagent (Takara Bio USA, San Jose, CA) was added, followed by an incubation at 37 °C for 2 h, and the absorbance at 450 nm was measured using a microplate reader (Biotek, EON, USA) as described [26].

2.8. RNA isolation and touchdown-quantitative real-time PCR (TqPCR)

Total RNA was isolated by using the TRIZOL Reagent (Invitrogen, China), and subjected to reverse transcription using hexamer and M-MuLV reverse transcriptase (New England Biolabs, Ipswich, MA). The cDNA products were used as PCR templates. Gene-specific PCR primers were designed by using Primer 3 program (Table S1). TqPCR was carried out by using 2x SYBR Green qPCR Master Mix (Bimake, Shanghai, China) on the CFX-Connect unit (Bio-Rad Laboratories, Hercules, CA) as described [40]. All TqPCR reactions were done in triplicate. *Gapdh* was used as a reference gene. Quantification of gene expression was carried out by using the $2^{-\Delta\Delta Cq}$.

2.9. Hyaluronic acid staining

Exponentially growing cells were seeded in 24-well plates at a density of 7000 cells per well. After 3 days, cells were gently washed with PBS, fixed with 4 % polyoxymethylene, and then stained with 1 % Alcian blue, pH = 2.5 for 5 min (Alcian Blue Cartilage Stain Kit, pH 1.0, G2541, Solarbio, China). The plates were washed with PBS and air-dried before photographed under a bright field microscope. The ECM also undergoes the same fixation and staining steps. Each assay condition was performed in triplicate.

2.10. Cell wound healing assay

The wound healing assay was conducted as previously described [41,42]. The imDFs infected with Ad-RFP or Ad-TGF-β1 were seeded in a 6-well plate and grown to full confluence. Wounds were created by scratching cells with a 10 μL pipette tip across the diameter of the well. The attached cells were gently washed with PBS and incubated in DMEM containing 10 % FBS. At the indicated timepoints, the wounds were photographed and measured using Image J software. The formula for calculating the wound healing rate (%) is (scratch width at 0 h - scratch width at 16 h)/scratch width at 0 h × 100 %. Each assay condition was performed in triplicate.

2.11. Transwell cell migration assay

Transwell assay was conducted as previously reported [41,43]. Transwell chamber filters were placed in a 24-well plate. 700 μL of medium containing 10 % FBS was added to the lower chamber, and 300 μL of FBS-free media containing 2×10^4 imDFs was added to the upper chamber. After 24 h, non-migrated cells in the upper compartment were removed, and the migrated cells on the underside of the chamber were fixed with 4 % paraformaldehyde. Subsequently, they were stained with a 0.5 % crystal violet/formalin solution and photographed under a light microscope. Each assay condition was performed in triplicate.

2.12. Cytoskeleton phalloidin staining

Exponentially growing imDFs were fixed with 4 % paraformaldehyde, treated with 0.5 % Triton X-100 for 10 min, washed with PBS, and then stained with YF® Dye/Rhodamine Phalloidin Conjugates. Cell nuclei were counterstained with DAPI (10 μg/mL) for 10 min at RT. Fluorescent images were captured using a laser confocal microscope (Leica TCS SP8). Each assay condition was performed in triplicate.

2.13. Preparation of dermal fibroblast-derived extracellular matrix (ECM)

The decellularized ECM was prepared as described [44]. The sterile 14 mm coverslips were placed in 24-well plates and coated with 0.2 % sterile gelatin for 60 min at 37 °C. After washing with PBS, the coverslips were cross-linked with 1 % sterile glutaraldehyde for 30 min at RT, and washed with PBS again. Cross-links were quenched by incubating with 1M sterile glycine in PBS for 20 min at RT and then rinsed in PBS. The coverslips were then incubated in medium (DMEM, 10 % FBS) for 30 min at 37 °C, rinsed with PBS and use immediately. 10,000 cells per well were cultured overnight. The next day, medium supplemented with 50 μg/mL of ascorbic acid was added to the wells to stimulate ECM secretion by the cells. The culture medium was replaced every two days. After ten days of culturing, the cells were removed by pre-warmed extraction buffer (20 mM NH_4OH, 0.5 % Triton X-100 in PBS). DNA residues were digested with 10 μg/mL of DNase I in PBS for 30 min at 37 °C. The matrix can be used immediately or stored in PBS containing 1 % antibiotic for up to 4 weeks at 4°C [45]. The structural characterization of the ECM was evaluated using IF staining and scanning electron microscopy (SEM) (JSM-IT700HR, Japan). The SEM images were subsequently processed

to assess the diameters of the fibers using ImageJ and Fiji software. Besides, three random Z-stack images of ECM were acquired for each COL3A1 IF stained sample, which were used to evaluate the thickness of ECM [45].

2.14. Degree of swelling

The degree of swelling was assessed as previously described [46]. Briefly, lyophilized ECM samples were weighed (=dry weight). After incubation in deionized water for 24 h, the samples were weighed again (=wet weight) and the degree of swelling was calculated using the following equation: Degree of swelling (%) = (wet weight − dry weight)/dry weight × 100 %.

2.15. Porosity analysis

The porosity of the ECM was estimated using liquid displacement as described [47]. The lyophilized ECM was first immersed in a known volume (v1) of water in a graduated cylinder. After 1 h, the total volume (including both the water and the ECM) was recorded as v2. The volume of water remaining in the cylinder after the removal of the ECM was recorded as v3. The porosity (%) of the ECM was calculated using the following formula: Porosity (%) = (v1 - v3)/(v2 - v3) × 100 %.

2.16. Cytotoxicity of 5 % GelMa hydrogel

The cytotoxicity of 5 % GelMa was evaluated using Calcein-AM/PI live/dead cell staining kits (Yeasen, Shanghai, China) and the WST-1 cell proliferation assay [26]. 1×10^6 iKera cells were seeded in 100 μL of 5 % GelMa (Aladdin, Shanghai, China, Lot#A2304431) hydrogel in 96-well plates. The mixture was then cross-linked with ultraviolet (UV) light for 30 s. Subsequently, 100 μL of 10 % FBS medium was added to each well, and the cells were cultured for 3, 5, and 7 days, respectively. Cells were incubated with the staining solution (1x buffer Assay Buffer: Calcein-AM: PI = 1000:1:3) at 37 °C for 1 h. Living cells (green) were observed, and fluorescent images were captured using a fluorescence microscope. Meanwhile, cell viability was quantitatively assessed using the WST-1 assay. In the control group, iKera cells were plated in a 96-well plate cultured in 10 % FBS medium.

2.17. Cytotoxicity of the ECM derived from imDFs

The cytotoxicity of ECM was evaluated using Calcein-AM/PI live/dead cell staining kits (Yeasen, Shanghai, China) and the WST-1 cell proliferation assay. Briefly, iKera cells and ECM were seeded in 96-well plates with 5 % FBS medium. After 24, 48, or 72 h, the cells were incubated with the staining solution (1x Assay Buffer: Calcein-AM: PI = 1000:1:3) at 37 °C for 1 h. Living cells (green) were observed, and fluorescent images were captured using a fluorescent microscope. Cell proliferation was quantitatively assessed using the WST-1 assay. In the control group, iKera cells were plated in 96-well plates cultured in 5 % FBS medium.

2.18. Acute local inflammatory response of ECM+5 % GelMa at the subcutaneous injection sites in mice

KM mice (female, 6 weeks old) were randomly divided into the ECM group (imDFs-ECM + 5 % GelMa) and the control group (5 % GelMa), with 9 mice in each group. 100 μL mixture was injected subcutaneously into the upper and lower sides of the mouse's back. Three mice were sacrificed at each time point (8h, 24h, and 72h) after injection, and tissues from the injection sites were collected for hematoxylin and eosin (H & E) staining and immunohistochemistry (IHC) analysis.

2.19. Tumorigenicity analysis of the imDFs in athymic nude mice

The imDFs-FLuc cells were stably transduced with the retroviral vector pSEB-FLuc, which expresses firefly luciferase, as described [19]. Exponentially growing imDFs-FLuc cells were injected subcutaneously into the flanks of athymic nude mice (6-week-old, male, 2×10^6 cells per injection, and 4 sites per mouse). The potential subcutaneous mass growth was evaluated at 3 and 30 days after implantation through whole-body bioluminescence imaging using the IVIS Lumina Series III In Vivo Imaging System (PerkinElmer, Waltham, MA). The acquired data were quantitatively analyzed using the Living Image Software (PerkinElmer) as described [42,48].

2.20. Full-thickness wounding experiment in vivo

A full-thickness wound model in mice was established as described [19,49]. Briefly, KM mice (6 weeks old male) were divided into different groups, and 3 mice per group. After the animals were anesthetized with isoflurane inhalation, the dorsal surface of each mouse was disinfected with 70 % alcohol, and a 1-cm diameter full-thickness incisional wound was created on the upper back of each mouse. In the PBS group, the wounds were treated with 100 μL PBS per mouse as a control. In the GelMa group, the wounds were treated with 100 μL of 5 % GelMa per mouse. In the GelMa + imDFs or iKera group, the wounds were treated with 100 μL of 5 % GelMa containing 2×10^6 cells per mouse. In the GelMa + imDFs-ECM group, the wound was initially treated with imDFs-ECM, followed by the application of 100 μL of 5 % GelMa, which was then cross-linked using UV light. In the GelMa + imDFs-ECM + iKera group, the wound was initially treated with imDFs-ECM and then covered with 100 μL of 5 % GelMa containing 2×10^6 iKera cells. The mice were administered antibiotics orally through their drinking water. Wound sizes were measured on days 0, 3, 7, 10, and 13, respectively. The extent of the wound damage was calculated using Image J. All the mice were euthanized on postoperative day 13. Wound beds were excised with a 1 cm margin of normal skin and fixed in 4 % paraformaldehyde for further histological analysis.

2.21. H & E, Masson's trichrome staining

The skin tissue Φ10mm centered on the healing site was retrieved, and the maximum diameter is longitudinally cut to observe the changes in the entire layer of skin at the healing center from mice at the endpoint. The retrieved wound healing samples were fixed with 4 % paraformaldehyde, embedded in paraffin, and sectioned along the maximum diameter. Serial sections were deparaffinized, rehydrated, and then underwent H & E, and Masson's trichrome staining by using the Masson's Trichrome Stain Kit (G1340, Solarbio, China) as described [26,50].

2.22. Immunohistochemical (IHC) staining

IHC staining was conducted by using the IHC staining kits (SP-9000, ZSGB-Bio, China) as described [26,50]. Briefly, the sections were deparaffinized, rehydrated, and subjected to antigen retrieval. After being blocked with 5 % BSA, the sections underwent immunostaining with primary antibodies against CD45 (1:100 dilution; Wanleibio; Cat# WL00922), CD54 (1:100 dilution; Wanleibio; Cat# WL02268), CD68 (1:100 dilution; Santa Cruz; Cat# sc-20060), CD206 (1:100 dilution; proteintect; Cat# 18704-1-AP), TGB-β1 (1:200 dilution; proteintect; Cat# 21898-1-AP) or COL1A1 (1:300 dilution; proteintect; Cat# 14695-1-AP). The biotin-labeled goat anti-rabbit IgG or anti-mouse IgG/streptavidin-HRP kit (SP-9000, ZSGB-Bio, China) was used to detect the proteins of interest. Sections incubated without primary antibodies were used as negative controls. The staining results were observed using a bright-field microscope (Leica, DM4B) and analyzed semi-quantitatively with ImageJ.

2.23. Visual dynamic detection of iKera cells implanted in wounds

A full-thickness wound model in mice was established as previously described. 2×10^6 iKera cells infected with recombinant adenovirus overexpressing green fluorescent protein (Ad-GFP) were mixed with 5 % GelMa and implanted into the wounds. Filter conditions and illuminations settings for GFP imaging were set an excitation/emission of 475/520 nm, high lamp level, medium binning, filter 1, and 1.0 s exposure time. Grayscale and fluorescent images of each sample were analyzed using Living Image software (IndiGO2).

2.24. Statistical analysis

All experiments were performed at least three times and/or repeated in three independent batches. Data were analyzed using GraphPad Prism 8 and presented as the mean ± standard deviation (SD). Statistical significance was confirmed using one-way analysis of variance and the student's t-test for comparing between groups. A value of $p < 0.05$ was deemed statistically significant.

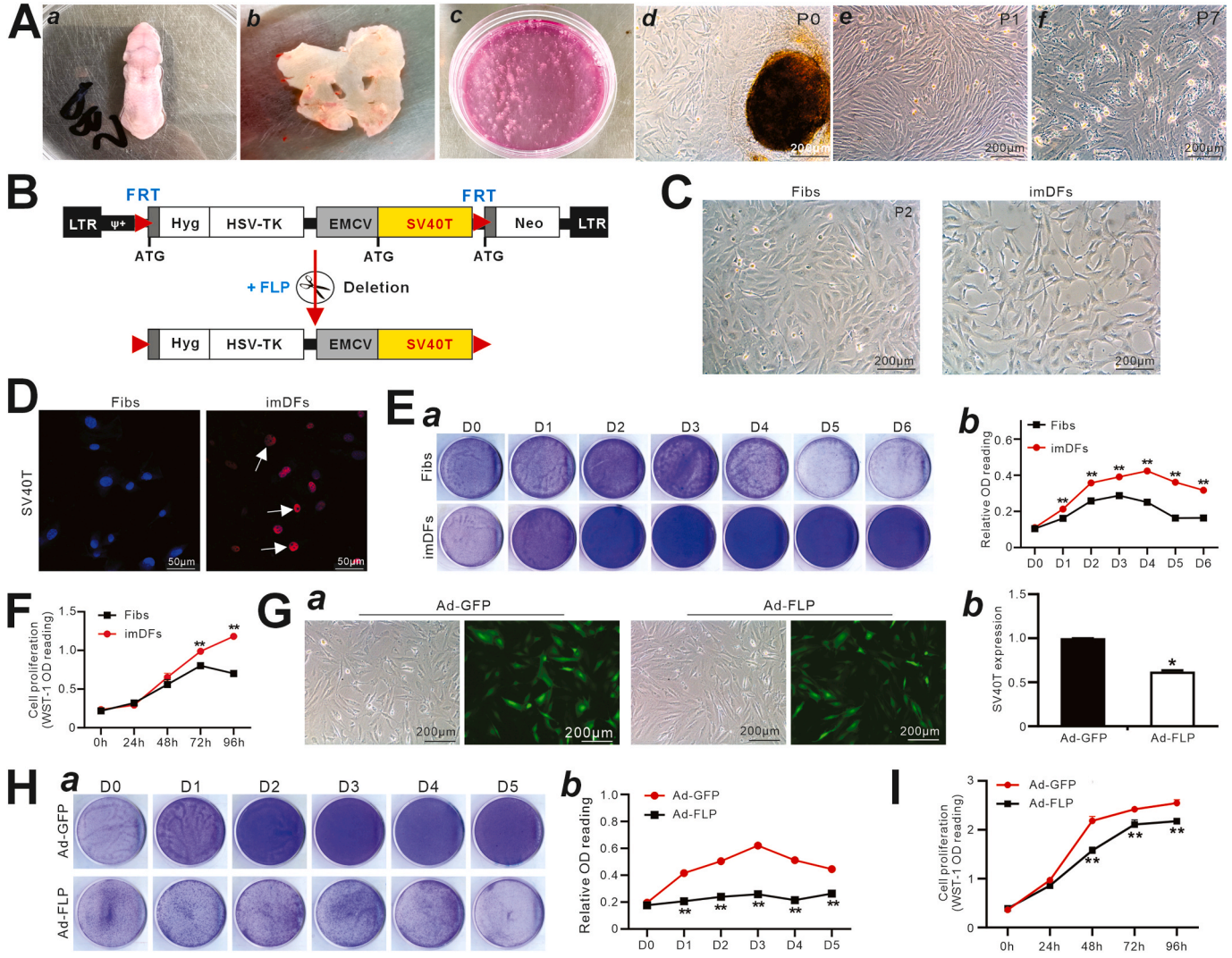

Fig. 1. Establishment of SV40 T-mediated reversibly immortalized mouse dermal fibroblasts (imDFs). (A) Steps for harvesting primary mouse dermal fibroblasts: (a) removal of lower forelimbs, hind limbs, and tail close to the body; (b) the freshly stripped skin tissues; (c) the cultured skin tissues after being minced into small pieces; (d) the recovered and proliferating primary dermal fibroblasts (Fibs) (P0); (e) primary dermal fibroblasts (P1); and (f) primary dermal fibroblasts (P7). (B) The schematic representation of SV40 T-mediated retroviral vector SSR#41. The SV40 T gene is flanked by FRT sites, enabling the removal of SV40 T upon the expression of FLP recombinase. (C) The morphologic comparison of Fibs (P2) and imDFs under phase contrast microscope. (D) Expression of SV40 T. Immunofluorescence (IF) staining was used to evaluate the expression and localization of SV40 T in Fibs (P1) and imDFs. The nuclei were counter-stained with DAPI. Representative positive stains were indicated by arrows. (E) Cell viability assay. Crystal violet staining assay (a) and quantitative analysis (b) were used to evaluate the viability and proliferation of Fibs (P7) and imDFs at days 0, 1, 2, 3, 4, 5, and 6. "**", $p < 0.01$, Fibs vs. imDFs at the indicated time points. (F) Cell proliferation assay. WST-1 assay was used to measure the cell proliferation of Fibs (P7) and imDFs at 0, 24, 48, 72, and 96 h, respectively. "**", $p < 0.01$, Fibs vs imDFs at the indicated time points. (G) Removal of SV40 T expression in imDFs. Subconfluent imDFs were infected with Ad-FLP or Ad-GFP, respectively, the fluorescence signals were recorded 36 h after infection (a). Total RNA was isolated for TqPCR analysis to assess the expression of SV40 T in imDFs 48 h after infection. "*", $p < 0.05$, Ad-FLP treated group vs Ad-GFP treated group (b). (H) Cell viability upon the removal of SV40 T in imDFs. Subconfluent imDFs were infected with Ad-FLP or Ad-GFP respectively. Crystal violet cell viability assay (a) and quantitative analysis (b) were utilized to evaluate the viability and proliferation of the imDFs at days 0, 1, 2, 3, 4 and 5. "**", $p < 0.01$, Ad-FLP treated group vs Ad-GFP treated group. (I) Effect of SV40 T removal on cell proliferation of imDFs. Subconfluent imDFs were infected with Ad-FLP or Ad-GFP, respectively. WST-1 assay was used to assess cell proliferation at 0, 24, 48, 72, and 96 h "**", $p < 0.01$, Ad-FLP treated group vs Ad-GFP treated group.

3. Results

3.1. Reversibly immortalized mouse dermal fibroblasts (imDFs) can be effectively established by stably expressing SV40 T antigen

To ensure a consistent supply of dermal fibroblasts for wound healing research, we sought to establish reversibly immortalized mouse dermal fibroblasts (imDFs). We first isolated primary dermal fibroblasts from neonatal mice, referred to as Fibs, following the procedure outlined in the Methods section (Fig. 1A–a to f). Since the SV40 large T antigen (SV40 T) is one of the most commonly used immortalizing genes, the retroviral vector SSR#41 [25,27,28,51–54], which expresses the hygromycin B resistance gene and SV40 T flanked by FRT sites, was used to create a reversible immortalized dermal fibroblast cell line, termed imDFs cells (Fig. 1B). Fibs (P2) and imDFs exhibited similar morphology *in vitro* (Fig. 1C). The expression of SV40 T in imDFs was verified through immunofluorescence (IF) staining in comparison with that in Fib cells (Fig. 1D, & Fig. S1A, and the negative control was shown in Fig. S1B). Unlike Fib cells, imDFs can be passaged and maintain high proliferative activity for at least 30 generations. We further demonstrated that imDFs exhibited a higher proliferation capacity and cell viability compared with Fib cells (P1) in the crystal violet cell viability assay (Fig. 1E) and the WST-1 assay (Fig. 1F). These results demonstrate that the SV40 T-mediated immortalization strategy can effectively transform Fib cells into long-term passage dermal fibroblast cell lines.

From a safety perspective, there are many uncertainties in transplanting immortalized cell lines with unlimited proliferation ability. Therefore, we attempted to construct reversible immortalized cell lines using the FLP-FRT system, and at an appropriate time, restore these immortalized cells to their original state. To investigate the reversibility of the immortalized phenotype of imDFs, we employed recombinant adenovirus expressing FLP recombinase (Ad-FLP) to knock out SV40 T. The imDFs were effectively transduced by both Ad-FLP and control Ad-GFP viruses (Fig. 1G–a). TqPCR analysis revealed a significant reduction

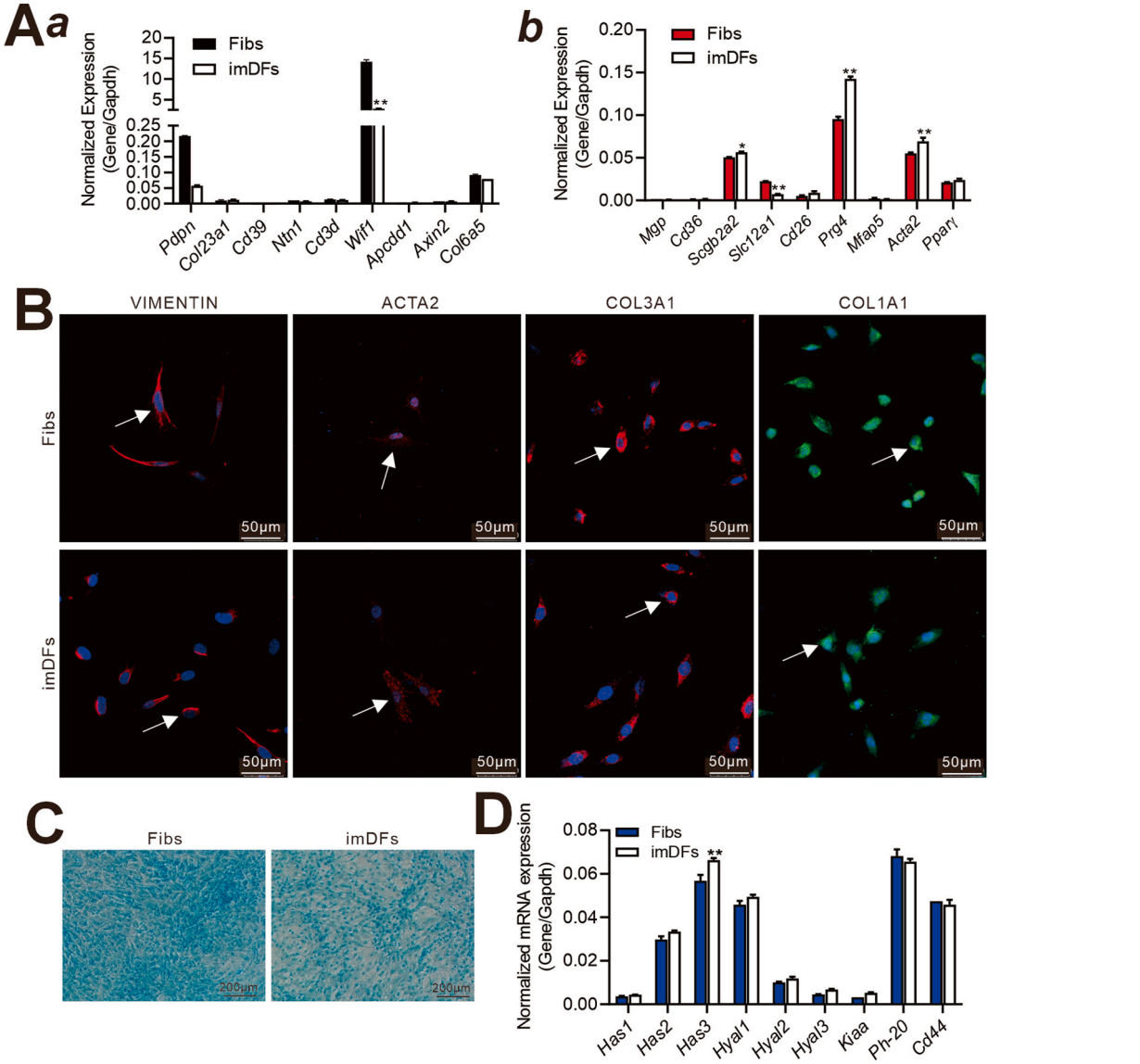

Fig. 2. Expression of characteristic skin markers and hyaluronic acid (HA) production of imDFs. (A) Total RNA was isolated from Fibs and imDFs for TqPCR analysis to assess the expression of papillary dermis (a) and reticular dermis (b) fibroblasts markers. "**", $p < 0.01$; "*", $p < 0.05$, Fibs vs imDFs. (B) IF staining was used to assess the expression and localization of VIMENTIN, ACTA2, COL3A1, and COL1A1 in Fibs and imDFs. The nuclei were counterstained with DAPI. Representative positive results were indicated by arrows. (C) The hyaluronic acid (HA) was stained with alcian blue in Fibs and imDFs. The blank cell slides were used as negative controls (NC). Representative positive results are shown. (D) Total RNA was isolated from Fibs and imDFs for TqPCR analysis to assess the expression of the genes involved in the synthesis and decomposition of HA. "**", $p < 0.01$, Fibs vs. imDFs.

in SV40 T expression in imDFs transduced with Ad-FLP compared to cells treated with the control virus (Fig. 1G–b). The results of the crystal violet cell viability (Fig. 1H–a & b) and WST-1 assays showed that the removal of SV40 T by Ad-FLP significantly reduced the proliferation rate of imDFs (Fig. 1I). Although SV40 T may be partially removed using the above method, these results strongly suggest that the SV40 T-mediated immortalization phenotype of imDFs may be reversed.

3.2. *The imDFs express characteristic markers of dermal fibroblasts, produce hyaluronic acid (HA) and are responsive to TGF-β1-induced transformation and activation*

The dermis is divided into a superficial papillary dermis and deeper reticular dermis [55]. We next conducted qPCR analysis and determined the expression of the well-established papillary dermis and reticular dermis fibroblast gene markers. The expression of most of papillary dermis fibroblast genes, particularly *Pdpn*, *Wif1*, and *Col6a5*, was easily detectable in both Fibs and imDFs (Fig. 2A–a). The expression of most of

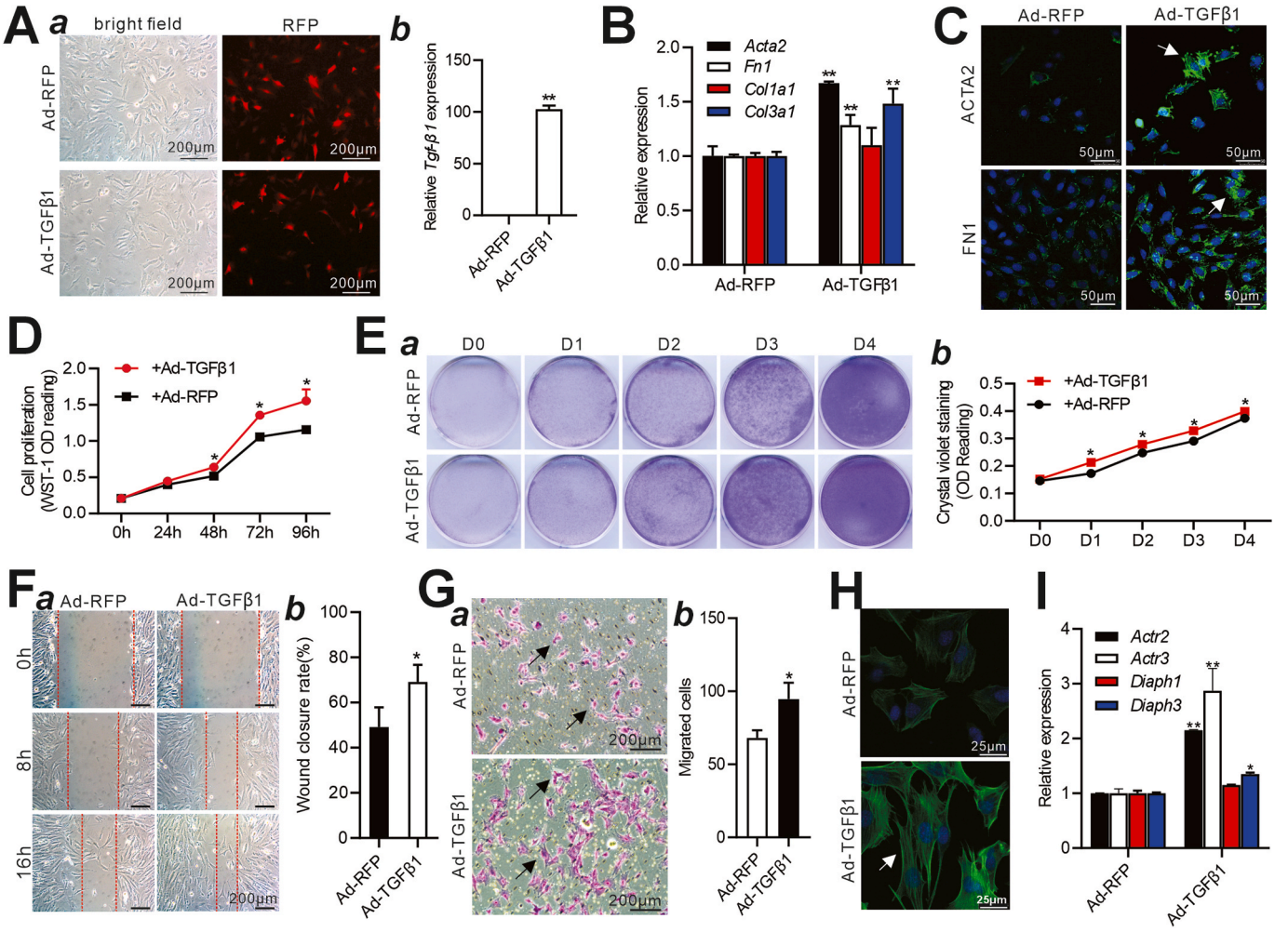

Fig. 3. Responsiveness to TGF-β1 by the imDFs. (A) Ad-TGFβ1 effectively transduces imDFs and mediates exogenous Tgf-β1 expression. Subconfluent imDFs were infected with Ad-TGFβ1 or Ad-RFP, respectively. The fluorescence signals were recorded 36 h after infection (*a*), and total RNA was isolated for TqPCR analysis to measure the expression of *Tgf-β1* in imDFs at 48 h after infection. "**", $p < 0.01$, Ad-TGFβ1 treated group vs Ad-RFP treated group (*b*). (B) Effect of TGF-β1 on myofibroblast markers of imDFs. Subconfluent imDFs were infected with Ad-TGFβ1 or Ad-RFP, respectively. TqPCR analysis was conducted to detect the expression of myofibroblast markers in imDFs 48 h after infection. "**", $p < 0.01$, Ad-TGFβ1 treated group vs Ad-RFP treated group. (C) Expression and location of ACTA2 and FN1 proteins of imDFs induced by TGF-β1. Subconfluent imDFs were infected with Ad-TGFβ1 or Ad-RFP, respectively. IF staining was used to assess ACTA2 and FN1 expression in imDFs at 72 h after infection, and the nuclei were counterstained with DAPI. Representative positive results were indicated by arrows. (D) Cell proliferation assay. Subconfluent imDFs were infected with Ad-TGFβ1 or Ad-RFP, respectively. WST-1 assay was used to assess cell proliferation of imDFs at 0, 24, 48, 72, and 96 h after infection. "*", $p < 0.05$ for the Ad-TGFβ1 treated group vs the Ad-RFP treated group. (E) Cell viability assay. Subconfluent imDFs were infected with Ad-TGFβ1 or Ad-RFP respectively. Crystal violet cell viability staining (*a*) and quantitative analysis (*b*) were used to evaluate the viability and proliferation of the imDFs at days 0, 1, 2, 3, and 4 after infection. "*", $p < 0.05$ for the Ad-TGFβ1 treated group vs the Ad-RFP treated group. (F) Cell migration/wound healing assay. Subconfluent imDFs were infected with Ad-TGFβ1 or Ad-RFP respectively. Wound healing assay (*a*) and the relative wound closure rates (%) (*b*) were analyzed at 0, 8, 16 h after infection. "*", $p < 0.05$, Ad-TGFβ1 treated group vs Ad-RFP treated group. (G) Cell migration/invasion assay. The transwell assay (*a*) and quantitative analysis were used to evaluate the cell migration of the imDFs at 24 h after infection. Positive staining migrated cells were indicated by arrows. "*", $p < 0.05$ for the Ad-TGFβ1 treated group vs. the Ad-RFP treated group. (H) Cytoskeleton staining. Subconfluent imDFs were infected with Ad-TGFβ1 or Ad-RFP respectively. The F-actin in cytoskeleton was stained with phalloidin at 48 h after infection, and the nuclei were counterstained with DAPI. Representative positive stain was indicated by an arrow. (I) Effect of TGF-β1 on cytoskeleton markers of imDFs. Subconfluent imDFs were infected with Ad-TGFβ1 or Ad-RFP respectively. The total RNA was isolated for TqPCR analysis of the expression of cytoskeletal motility-related genes, *Actr2, Actr3, Diaph1*, and *Diaph2* in imDFs. "**", $p < 0.01$; "*", $p < 0.05$, Ad-TGFβ1 treated group vs. Ad-RFP treated group.

reticular dermis fibroblast genes, particularly *Scgb2a2, Prg4, Acta2,* and *Pparγ,* was also easily detectable in both Fibs and imDFs (Fig. 2A–b). IF staining analysis further confirmed the high expression of fibroblast protein VIMENTIN, COL3A1and COL1A1, and low expression of ACTA2 in Fibs and imDFs (Fig. 2B, & Fig. S1A).

Hyaluronic acid (HA), a non-sulfated glycosaminoglycan (GAG), is a major component of skin extracellular matrix (ECM) that is secreted by dermal fibroblasts and involved in the inflammatory response, angiogenesis, and tissue regeneration process [56]. Dermal fibroblasts are also the main secretory cells of hyaluronic acid in the skin. We further observed a large amount of HA was produced both in Fibs and imDFs cells by Alcian blue staining (Fig. 2C, and the negative control was shown in Fig. S1C). The expression of hyaluronan synthase genes, Has1, Has2, Has3, hyaluronic acid lyase and related genes, Hyal1, Hyal2, Hyal3, Kiaa, Ph-20 and Cd44 was readily detectable in both Fibs and imDFs (Fig. 2D).

It has been reported that dermal fibroblasts can transform into myofibroblasts upon stimulation by TGF-β1[1,57,58]. Recombinant adenoviruses expressing TGF-β1 (Ad-TGFβ1) and RFP (Ad-RFP) were used to infect imDFs, and TqPCR analysis indicated that TGF-β1 expression was significantly upregulated in the imDFs transduced with Ad-TGF-β1, compared with that treated with the control viruses (Ad-RFP) (Fig. 3A). Upon conducting qPCR analysis, we detected upregulated levels of myofibroblast markers, Acta2, Fn1 and Col3a1 in imDFs cells from the Ad-TGFβ1 group compared with Ad-RFP treated group (Fig. 3B). IF experiments further demonstrated that imDFs in the Ad-TGFβ1 group upregulated the expression levels of ACTA2 and FN1 proteins (Fig. 3C, & Fig. S1D). In addition, the WST-1 assay and crystal violet cell viability assay also showed that TGF-β1 could promote the proliferation and viability of imDFs (Fig. 3D & E). The results of the wound healing assay and chamber assay demonstrated that TGF-β1 could enhance the migration ability of imDFs (Fig. 3F & G). Cytoskeletal staining and mRNA levels of cytoskeletal motility-related genes indicated TGF-β1 promotes imDF migration ability by affecting cytoskeletal

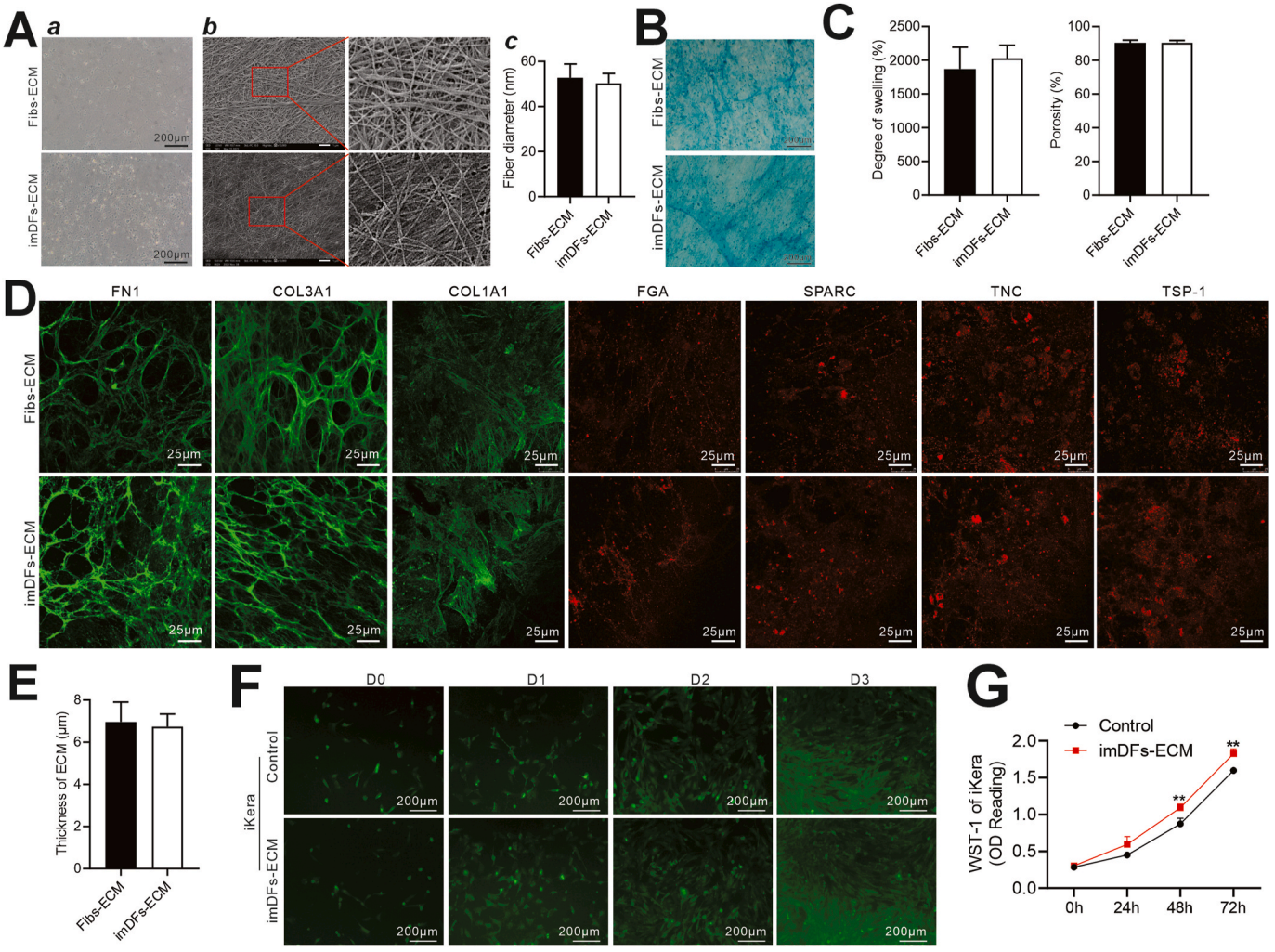

Fig. 4. Characterization of decellularized ECM derived from imDFs (imDFs-ECM). The ECM was prepared as described in Method. (A) Morphology and appearance of ECM. The ultrastructure of the ECM derived from Fibs and imDFs (designated as Fibs-ECM and imDFs-ECM respectively) was assessed using light microscope (*a*) and scanning electron microscopy (SEM) (*b*). Representative images are shown. Fiber diameter was counted based on SEM results as described. (B) The HA was stained with alcian blue in Fibs-ECM and imDFs-ECM. Representative positive results are shown. (C)The swelling rate and porosity of Fibs-ECM and imDFs-ECM were evaluated. (D) Detection of major protein components of extracellular matrix. IF staining was used to assess the expression of FN1, COL3A1, COL1A1, FGA, SPARC, TNC, and TSP-1 in the Fibs-ECM and imDFs-ECM. FN1, COL3A1 and COL1A1 were shown by green fluorescence, FGA, SPARC, TNC, and TSP-1 were shown by red fluorescence. Representative images are shown. (E) The thickness of Fibs-ECM and imDFs-ECM based on IF staining of COL3A1. (F) Cytotoxicity of ECM. Subconfluent iKera cells were cultured with imDFs-ECM, and iKera cells were stained with Calcein-AM/PI to assess the cytotoxicity of ECM at days 0, 1, 2, and 3. Living cells were shown in green fluorescence. iKera cells in 5 % FBS DMEM was set as the control. (G) Cell proliferation assay. Subconfluent iKera cells were cultured with imDFs-ECM, and WST-1 was used to assess cell proliferation at 0, 24, 48 and 72 h. iKera cells in 5 % FBS DMEM was set as the control. "**", $p < 0.01$, ECM group vs. Control group.

architecture (Fig. 3H & I). In conclusion, based on the above cell function experiments, we believe that imDFs cells exhibit similar biological characteristics to primary dermal fibroblasts.

3.3. The imDFs-derived extracellular matrix (imDFs-ECM) maintains similar 3D structure and protein components to that of the ECM derived from primary dermal fibroblasts, and exhibits low cellular and tissue toxicity

The ECM is an acellular, protein-rich matrix that is secreted by dermal fibroblasts, and provides structural support and cellular attachment in wound healing by directly modulating many aspects of cell behaviors including adhesion, proliferation, migration, and survival. The ECM can indirectly modulate cells and regulate extracellular protease secretion and growth factor bioavailability [59]. We prepared the Fibs or imDFs-derived ECM as described above and observed ECM under the microscope (Fig. 4A, panel a). Microarchitecture analysis by scanning electron microscopy (SEM) showed that the ECM samples were composed of a dense meshwork of filaments and the fiber diameter was approximately 50 nm both in Fibs-ECM and imDFs-ECM (Fig. 4A, panel b & c, the low magnification field of view was shown in Fig. S1E and the negative control was shown in Fig. S1F). Alcian blue staining results showed that Fibs-ECM or imDFs-ECM were rich in HA (Fig. 4B). The swelling rate was around 2000 % and the porosity was about 90 % both of Fibs-ECM and imDFs-ECM (Fig. 4C). The high swelling degree and porosity provide space for cell growth and angiogenesis, while implying a decrease in mechanical strength. When the key protein components of ECM were stained by IF, we observed a high expression level of FN1, COL3A1 and COL1A1, and a low expression level of FGA, SPARC, TNC and TSP-1 [60–62] in Fibs-ECM and imDFs-ECM (Fig. 4D). The thickness of ECM was approximately 7 μm both in Fibs-ECM and imDFs-ECM (Fig. 4E). The above results indicate that the structure and key protein compositions are very similar in the ECM derived from Fibs and imDFs.

In order to ensure that imDFs-ECM can firmly cover the skin wound in subsequent animal models, we mixed the stretched imDFs-ECM in 5 % GelMa hydrogel. Methacrylated gelatin (GelMa) is a double bond modified gelatin that can be crosslinked and cured into a gel by UV and visible light under the action of a photoinitiator. GelMa combines the characteristics of natural and synthetic biomaterials, with a three-dimensional structure suitable for cell growth and differentiation, excellent biocompatibility, and cellular response properties. The 5 % GelMa hydrogel has good tissue adhesion and solid morphology that were verified in our previous study [26]. We next analyzed the viability of the inoculated cells in the 3D microenvironment. Calcein AM/PI staining and WST-1 assays shown that iKera cells survived and proliferated in 5 % GelMa (Fig. S1G), consistent with our previous studies [26]. Calcein AM/PI staining also showed that imDFs-ECM had almost no cytotoxic effect on iKera cells (Fig. 4F). In fact, the WST-1 assay revealed that the imDFs-ECM enhanced iKera cell proliferation (Fig. 4G).

Studies have shown that ECM and GelMa do not cause acute or chronic immune reactions [63,64]. We also analyzed the potential host immune response and hypersensitivity induced by subcutaneous injection of imDFs-ECM. We found that subcutaneous injection of imDFs-ECM+5 % GelMa into immune-competent mice did not cause significant skin papules (Fig. 5A). In H & E staining, we observed that imDFs-ECM induced capillary dilation at 8h, and aggregated inflammatory cells at 24h, which disappeared at the treatment sites 72h after injection. Since mature dendritic cells (DC) are important antigen-presenting cells that activate T lymphocytes and regulate acute immune responses, IHC staining revealed that the inflammatory cells (marked by CD45), mature DCs (marked by CD54), and macrophages (marked by CD68 and CD206) generated and aggregated towards to the injection point 24h after injection at the subdermal injection site. However, the numbers of these inflammatory cells significantly decreased and almost returned to normal levels at 72h after injection (Fig. 5B & Fig. S2A). Interestingly, the accumulation of both CD68 (inflammatory) and CD206 (anti-inflammatory) macrophages, suggesting a simultaneous inflammatory and anti-inflammatory response. Macrophage polarization is intricately regulated by cytokines, chemokines, and metabolites present in the surrounding microenvironment. For instance, signals such as IFN-γ and LPS promote M1 polarization, while IL-4 and IL-13 induce M2 polarization [45,65]. The diversity and abundance of endogenous signaling molecules within the ECM—such as growth factors, cytokines, cryptic peptides, and microRNAs—are likely significant contributors to this phenomenon. Additionally, the coexistence of M1 and M2 macrophages is essential for immune homeostasis. Excessive M1 activity can lead to tissue damage and chronic inflammation [66], while predominant M2 activity may weaken immune defenses or promote pathogen growth. Therefore, their coexistence represents a crucial mechanism for maintaining balance at a wounded site. These results indicate that the imDFs-ECM elicits a very short period of host inflammatory response and exhibits extremely low cellular and tissue toxicity, suggesting that the tested imDFs-ECM may serve as a generic biomaterial scaffold.

3.4. imDFs and imDFs-ECM can both promote the healing of skin wounds in vivo

The nude mouse ectopic tumorigenesis test is currently a highly recognized method for identification of tumor cells *in vivo* [67,68]. Due to congenital thymic defects in nude mice, they are unable to produce T lymphocytes, allowing tumorigenic cells injected subcutaneously to escape the killing of T lymphocytes and rapidly proliferate to form tumors. Tumorigenic cells generally begin to form measurable tumors within 7–10 days, which grow significantly over the subsequent weeks. Depending on the type of tumor cells and treatment conditions, tumor volumes typically reach between 1000 and 3000 mm^3 within 3–6 weeks [69]. We further tested whether imDFs are tumorigenic by injecting the firefly luciferase-tagged imDFs (imDFs-FLuc) subcutaneously in athymic nude mice. Whole-body bioluminescence imaging analysis revealed that the bioluminescence signal was readily detected at day 3 after injection, and essentially disappeared 30 days after injection. No subcutaneous tumor formation was observed after 60 days (Fig. 6A), demonstrating that the imDFs are not tumorigenic.

To test the effect of imDFs and imDFs-ECM on skin wound healing, we established an experimental mouse skin wound healing model and applied the cells or imDFs-ECM to the wound as described above. No signs of inflammation or infection were observed during the healing process in all groups (Fig. 6B, panel a). The wound healing process was accelerated most significantly in the GelMa + imDFs-ECM group, and to a lesser extent in the GelMa + imDFs group, starting as early as at day 3 (Fig. 6B, panel b). Since the presence of hair follicles, sweat glands, sebaceous gland and other skin appendages is considered as components of newly healed skin, H & E staining indicated that the diameter of the unhealed skin wound was the shortest in the GelMa + imDFs-ECM group, and at the healing center new tissues were found protruding from the surrounding skin plane in the GelMa + imDFs-ECM group and the GelMa + imDFs group (Fig. 6C left columns). Masson's trichrome staining revealed that more collagen fibers were produced in the dermis layer in the GelMa + imDFs-ECM group and the GelMa + imDFs group, compared with that in in the PBS group and GelMa group (Fig. 6C, right columns). The Scar Elevation Index (SEI) was used to quantify scar formation based on Masson's trichrome staining results (Fig. 6D). These results showed that the healing sites of imDFs and imDFs-ECM groups protrude from the skin surface. During the remodeling phase of wound healing, newly synthesized COL3A1 begins to degrade, while mature COL1A1 increases, thereby enhancing the mechanical strength of the skin. However, excessive production of COL1A1 is often linked to hypertrophic scarring [70,71]. IHC staining revealed that COL1A1 expression was significantly higher in the imDFs and imDFs-ECM groups (Fig. 6E). The above results strongly suggest that imDFs and imDFs-ECM

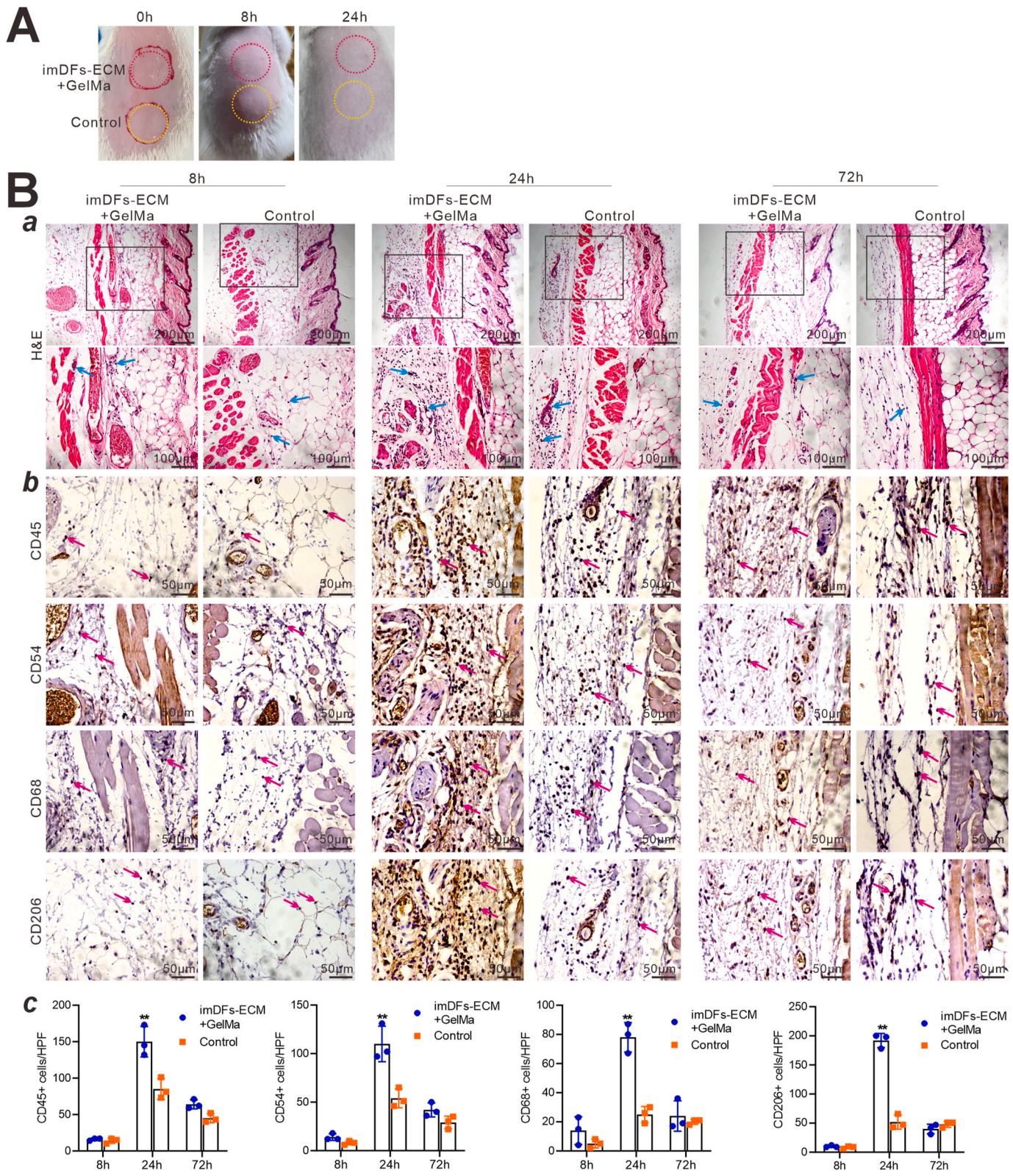

Fig. 5. Biocompatibility of imDFs-ECM *in vivo*. (A) ECM-induced inflammation assessment *in vivo*. KM mice were subcutaneously injected with imDFs-ECM in 5 % GelMa (namely imDFs-ECM + GelMa in yellow ring) and observed at 8, 24, and 72 h after injection. Equal volume 5 % GelMa was set as a control. (B) Histological evaluation and IHC staining. The skin tissues from Φ1.0 cm centered on the injection sites were retrieved. The inflammatory cells were indicated by blue arrows in H & E staining (*a*). IHC staining was used to detect the expression of CD45, CD54, CD68, and CD206. Positive staining cells were indicated by red arrows (*b*) and the number of positive cells in a random field of view is quantified (*c*).

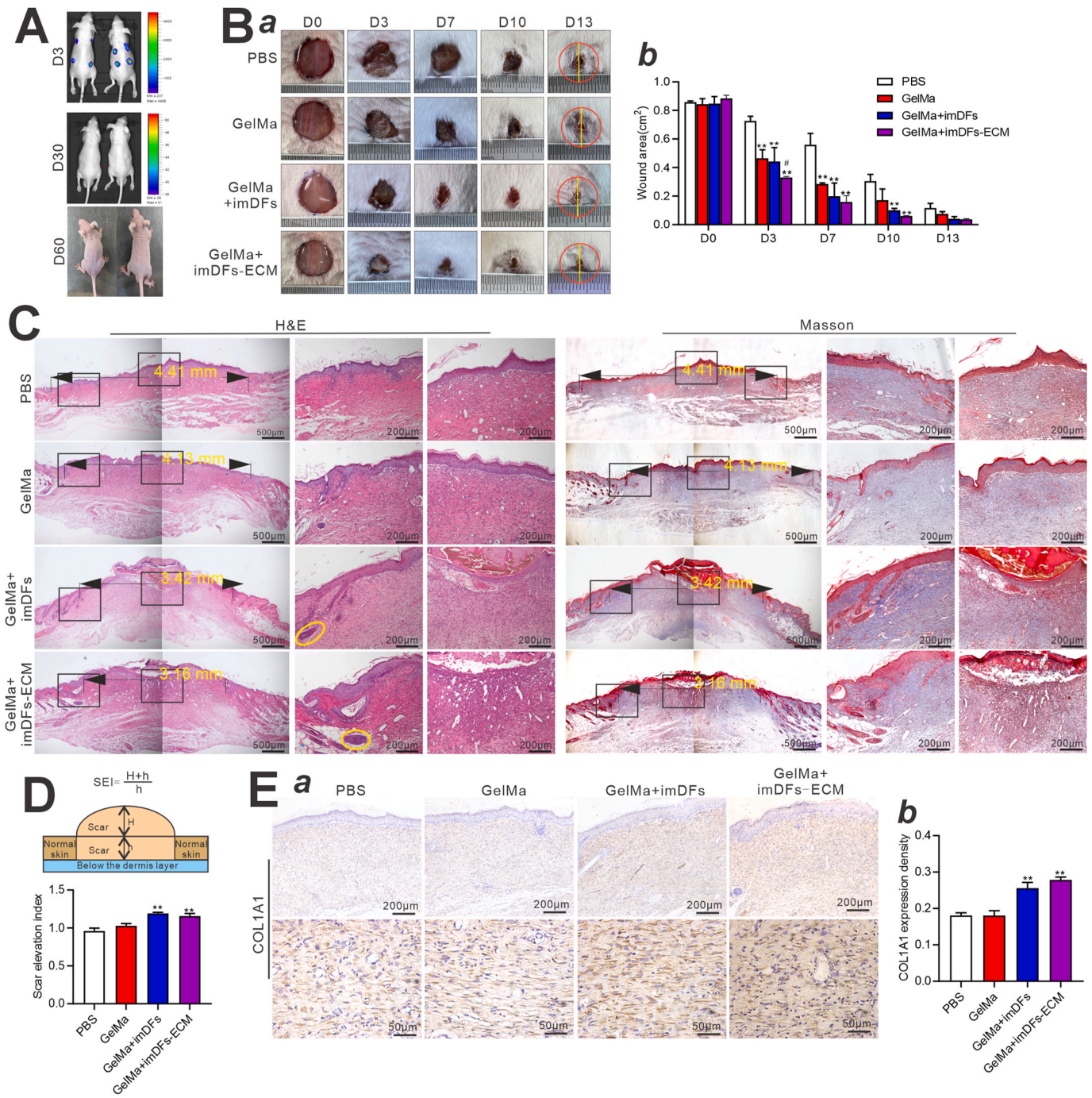

Fig. 6. The imDFs-ECM accelerates skin wound healing. (A) imDFs are non-tumorigenic. Subconfluent imDFs stably expressing firefly luciferase (imDFs-FLuc) were subcutaneously injected into the flanks of athymic nude mice. The animals underwent Xenogen IVIS 200 whole-body bioluminescence imaging on days 3 and 30, and directly observed the appearance of nude mice after 60 days. Representative images are shown. (B) The effects of the imDFs or imDFs-ECM combined with 5 % GelMa on skin wound healing. A Φ1cm full-thickness skin wound was created on the dorsal part of each mouse. The operated mice were divided into four groups: PBS group (PBS), 5 % GelMa group (GelMa), 5 % GelMa + imDFs group (GelMa + imDFs), and 5 % GelMa + imDFs-ECM group (GelMa + imDFs-ECM), and the initial dimensions of skin wounds were measured and recorded on days 0, 3, 7, 10, and 13 (a). "**", $p < 0.01$ for the GelMa group, GelMa + imDFs group, or GelMa + imDFs-ECM group vs. the PBS group at respective time points. "#", $p < 0.05$ for the GelMa + imDFs-ECM group vs. the GelMa group at respective time points (b). (C) As shown in Fig. 6B, the skin tissue Φ10mm centered on the healing site was retrieved (red circular), and the maximum diameter (yellow line) is longitudinally cut to observe the changes in the entire layer of skin at the healing center from mice at the endpoint. Histological assessment of the wound-healing process in the four groups. The skin tissues from Φ0.5 cm centered on wound were subjected for histological assessment by H & E staining and Masson's trichrome staining. Sebaceous glands were indicated with yellow ring, and the subcutaneous adipose tissue was indicated with blue * in H & E staining. Masson staining was used to reveal the epidermal fibers in the epidermis layer (stained red) and the collagen fibers in dermis layer (stained blue). (D) Quantitative analysis of skin scar risk at the healing site using Scar Elevation Index (SEI) based on Masson's trichrome staining in Fig. 6C. (E) IHC staining of COL1A1 in all groups (*a*), and semi-quantified by Image J (*b*).

may significantly accelerate wound healing with excessive collagen production in the dermis, increasing the risk of hypertrophic scarring.

3.5. The combined application of iKera cells and imDFs-ECM results in scarless wound healing

The above results indicate that even though imDFs-ECM may be beneficial for skin wound healing, the direct use of imDFs was shown to promote fibrotic healing with a high risk of hypertrophic scarring. Numerous studies have shown that during the healing process of wounds, dermal fibroblasts proliferate extensively and secrete a large amount of extracellular matrix, which together with newly formed capillaries forms granulation tissue to fill the wound and provide conditions for the re epithelialization of keratinocytes [72,73]. Using our recently immortalized mouse keratinocyte cell lines (iKera) [19], we tested whether a combined use of keratinocytes and imDFs-ECM would promote scarless wound healing. The conditioned medium prepared from iKera cells was shown to enhance the proliferation and viability of imDFs based on the WST-1 assay (Fig. 7A) and the crystal violet cell viability assay (Fig. 7B).

Whole-body imaging analysis revealed that the GFP signal was readily detected at day 8 after implanting iKera cells (labeled with green

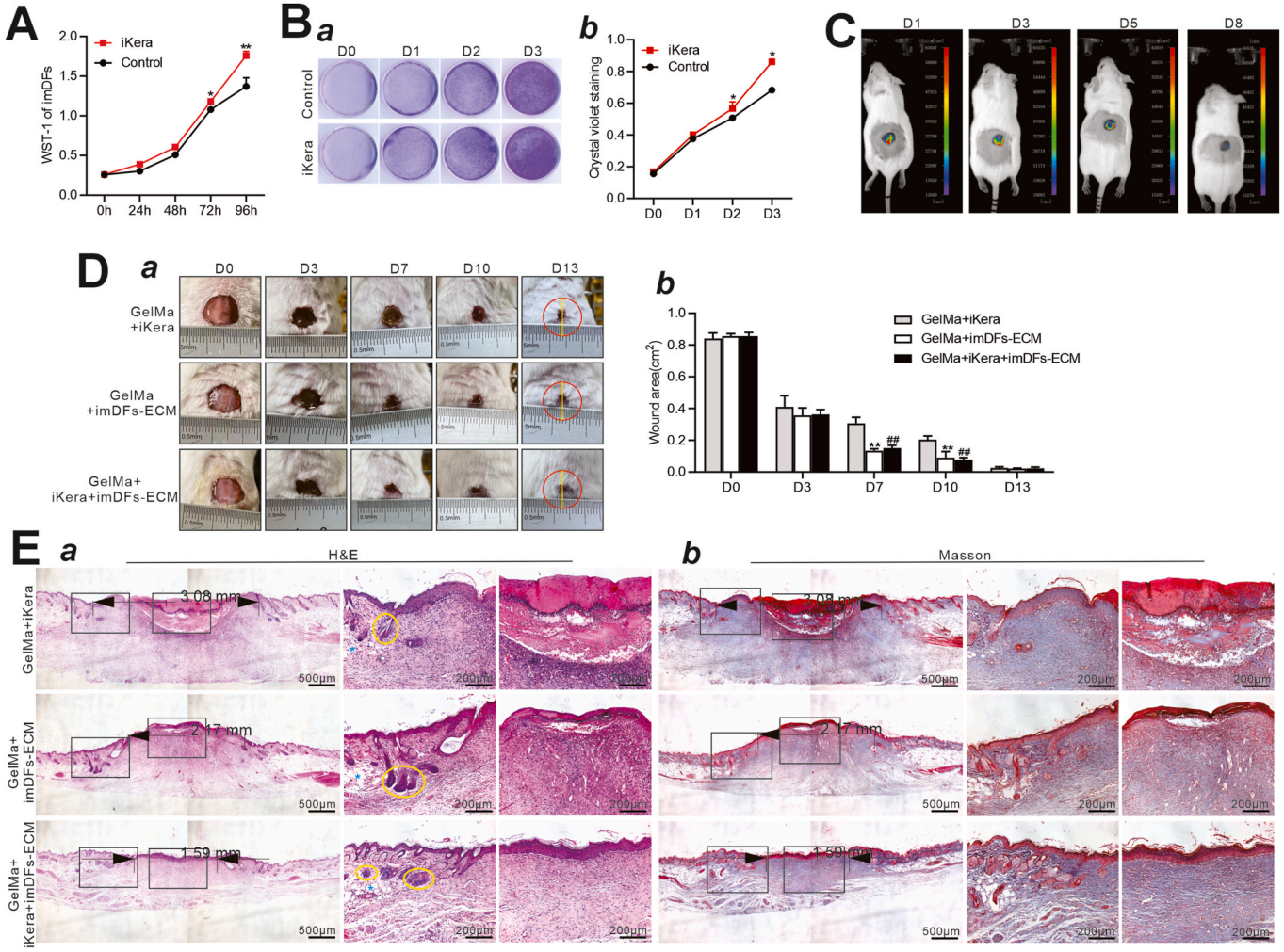

Fig. 7. The imDFs-ECM synergizes with iKera cells in promoting re-epithelization and scarless wound healing of skin injury. (A) The effect of iKera cells on the proliferation of imDFs. Subconfluent imDFs were cultured with the conditioned medium of iKera cells (iKera group). The cells in control group received the same cell-free culture medium. WST-1 assay was used to evaluate the proliferation of imDFs at 0, 24, 48 and 72 h "**", $p < 0.01$; "*", $p < 0.05$, the iKera group vs. the control group. (B) Cell viability affected the conditioned medium of iKera cells. Subconfluent imDFs were cultured with conditioned medium prepared from iKera cells, and the crystal violet cell viability staining (*a*) and quantitative analysis (*b*) were used to evaluate the viability and proliferation of the imDFs. "*", $p < 0.05$, the iKera group vs. the control group. (C) Exogenous iKera cell in wound. 2×10^6 iKera cells infected with Ad-GFP were mixed with 5 % GelMa and implanted into wounds as described in method. The animals underwent whole-body imaging on days 1, 3, 5 and 8. (D) The *in vivo* effect of the iKera cells combined with ECM on skin wound healing. A Φ1cm full-thickness skin wound was created on the dorsal part of each mouse. The operated mice were divided into three groups: 5 % GelMa + ikera cells group (GelMa + iKera), 5 % GelMa + imDFs-ECM group (GelMa + imDFs-ECM), and 5 % GelMa + ikera cells + imDFs-ECM (GelMa + iKera + imDFs-ECM) (*a*), and the initial dimensions of skin wounds were measured and recorded on days 0, 3, 7, 10, and 13 (*b*). "**", $p < 0.01$ for the GelMa + imDFs-ECM group vs. the GelMa + iKera group at respective time points, while "##", $p < 0.01$, the GelMa + ikera + imDFs-ECM group vs. the GelMa + iKera group. (E) As shown in Fig. 7D, the skin tissue Φ1cm centered on the healing site was retrieved (red circular), and the maximum diameter (yellow line) is longitudinally cut to observe the changes in the entire layer of skin at the healing center from mice at the endpoint. Histological assessment of the wound-healing process in the three groups. The skin tissues from Φ0.5 cm centered on the wound were retrieved at 13 days after injury and subjected for histological assessment. The sebaceous glands were indicated with yellow ring, and the subcutaneous adipose tissue was indicated with blue * in H & E staining (*a*). Masson's trichrome staining was used to reveal the epidermal fibers in the epidermis layer (red staining) and the collagen fibers in dermis layer (blue staining) (*b*). Field views of the healed wound with lower magnification are shown in the left column. Higher magnification of the two boxed areas indicating the edge and the center of the wounds is shown in the right columns. Representative images are shown.

fluorescent protein) with 5 % GelMa hydrogel directly (Fig. 7C). We further created a full-thickness skin defect model, and applied the GelMa hydrogels mixed with iKera cells, imDFs-ECM or imDFs-ECM + iKera cells to the skin wounds. While no signs of inflammation or infection were observed during the healing process in any of the groups, the GelMa + imDFs-ECM group and GelMa + iKera + imDFs-ECM group yielded smaller wound areas than that in the GelMa + iKera group at as early as day 6 post treatment (Fig. 7D, panels *a & b*).H & E staining analysis revealed that the unhealed skin defect diameter was the shortest in the GelMa + iKera + imDFs-ECM group among all groups. Furthermore, the healing surface in the GelMa + ikera + imDFs-ECM group consisted of a flat and smooth contour without any apparent protrusions and covered with a thin epithelial layer (Fig. 7E, panel *a*). Masson's trichrome staining revealed that the collagen fibers at the unhealed skin defect were arranged in a more organized fashion in the GelMa + iKera + imDFs-ECM group than that in the other groups (Fig. 7E, panel *b*).

SEI based on Masson's trichrome staining results are shown in Fig. 8A, panel *b*. These results showed that the healing sites of imDFs-ECM group protrude from the skin surface, and demonstrate that iKera cells may reduce the risk of scar formation. TGF-β1 plays a key role in the proliferative phase of wound healing by promoting the migration and proliferation of fibroblasts and keratinocytes, the formation of granulation tissue, as well as collagen synthesis and angiogenesis. However, in the late stage of wound healing, activation of TGF-β1 stimulates excessive proliferation of dermal fibroblasts, leading to scar formation [74,75]. Keratinocytes can downregulate TGF-β1 expression in fibroblasts during skin healing, this is beneficial for the scarless healing of wounds [76]. We conducted IHC staining analysis and found that TGF-β1 was highly expressed in the newly formed epidermal layers of all three groups, while its expression was lower in the dermal layer of the GelMa + iKera group and GelMa + iKera + imDFs-ECM group (Fig. 8B). The negative controls were shown in Fig. S2B. Collectively, the above results demonstrate that a combination of the dermal fibroblast-derived ECM and keratinocytes can significantly facilitate wound healing and re-epithelialization, while reducing the risk of scar formation.

4. Discussion

The crosstalk between epidermal keratinocytes and dermal fibroblasts is critical for skin homeostasis and wound healing [17,18]. In this study, we used the reversibly immortalized dermal fibroblasts imDFs as the surrogate cell source of primary dermal fibroblasts. The immortalization phenotype of the imDFs can be reversed by FLP recombinase, whereas *in vivo* experiments demonstrated that the imDFs were not tumorigenic in athymic nude mice. The expression of the well-established dermal fibroblast gene markers in the imDFs were readily detected at similar levels to that in primary dermal fibroblasts. In particular, we found that Vimentin, Col1a1, and Col3a1 in the imDFs were expressed at comparable levels with that of primary dermal fibroblasts. As expected, imDFs express a low level of Acta2 that is highly expressed in smooth muscle cells and myofibroblasts [2]. We also found that a large amount of hyaluronic acid was produced, and the expression of hyaluronan synthase genes was readily detectable in both primary dermal fibroblasts and imDFs, as hyaluronic acid is known to accelerate re-epithelialization and healing of acute cutaneous wounds [77]. Since dermal fibroblasts can transform into myofibroblasts upon by TGF-β1 stimulation [1,57,58], we found that expression levels of myofibroblast markers, Acta2, Fn1 and Col3a1 were significantly up-regulated by TGF-β1 in imDFs, and that TGF-β1 enhanced the migration ability of imDFs. Thus, our experimental findings demonstrate that imDFs exhibit biological characteristics similar to that of primary dermal fibroblasts. Nonetheless, dermal fibroblasts are heterogeneous populations derived from early embryonic dermal fibroblast progenitors, which can differentiate into several cell types such as upper papillary fibroblasts, lower reticular fibroblasts, dermal condensate/dermal papilla, and intradermal adipocytes/dermal white adipose tissue [6,78]. The imDFs were primarily isolated from the dermis and may not include all subpopulations of dermal fibroblasts. Our *in vivo* experiments demonstrate that the imDFs promoted fibrotic wound healing, indicating that the supply of fibroblasts alone may lead to an over-production of ECM and fibrosis.

ECM not only plays an important role during development [79,80], but also is a critical factor in wound healing [59,81,82]. ECM is a complex, heterogeneous network of soluble and insoluble molecules that provides a physical structure that is essential for cell adhesion, growth, and differentiation [8], as well as biochemical milieu for cells to interact with through integrins. It was reported that an ECM glycoprotein TGFBI located in the basement membrane enhanced the growth and function of epidermal stem cells (EpSCs) and promoted wound healing [83]. Epidermal maintenance relies on the integrin-mediated anchoring of basal epidermal stem cells to the lower dermis through extracellular matrix proteins [9]. Furthermore, ECM acts as a reservoir for growth factors, binding and regulating their bioavailability [12]. Many growth factors, such as FGF and VEGF, tightly bind to heparin and heparan sulfate, which are components of many ECM proteoglycans [10,11], while growth factors can be released from the ECM by degrading ECM

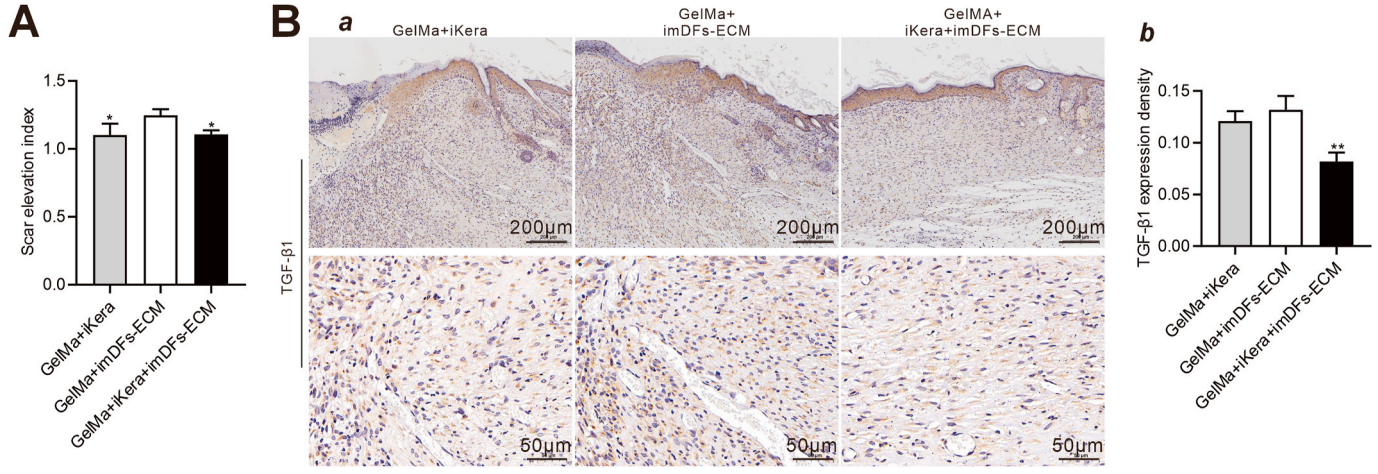

Fig. 8. Expression of TGF-β1 at the skin wound healing sites. (A) SEI based on Masson's trichrome staining in Fig. 7E, panel b. "*", $p < 0.05$ for the GelMa + iKera group or GelMa + iKera + imDFs-ECM group vs. the GelMa + imDFs-ECM group. (B) The retrieved skin samples in Fig. 7D were subjected to IHC staining for TGF-β1 (*a*), and the semi-quantitative analysis of IHC staining of TGF-β1 in healing center of dermis layer by Image J. "**", $p < 0.01$ for the GelMa + imDFs-ECM group vs. the GelMa + iKera + imDFs-ECM group (*b*).

proteins or glycosaminoglycan components of proteoglycans [10].

Emerging evidence reveals that ECM-based biomaterials have become promising scaffolds for generative medicine and other clinical translation applications [80,84,85]. It was reported that ECM derived from induced pluripotent stem cells was used to create biological scaffold materials for *in vitro* models of diabetic wound healing [15]. Human lung fibroblast-derived matrices (hFDM) that were used to create 3D vascular structures loaded with growth factors and transplanted with human umbilical vein endothelial cells (HUVECs) in a wound model were shown to be more effective in re-epithelialization and regenerated hair follicles with more advanced neovascularization [16]. In our study, using a full-thickness skin defect model we found that imDFs-derived ECM delivered with GelMA hydrogel promoted more effective wound healing than the control group, although H & E staining and Masson's trichrome staining revealed that re-epithelialization of the healed wounds were rather limited in the ECM treated group, suggesting that keratinocytes may be added to facilitate the re-epithelialization.

To explore potential solutions, we investigated the effect of adding keratinocytes, in addition to ECM, on wound healing. We previously demonstrated that incorporating keratinocytes (i.e., iKera) on the wound surface enhance re-epithelialization [19]. Following a similar approach, we created a full-thickness skin defect model and treated the wound with the GelMA hydrogel of iKera and imDFs-derived ECM mix. We found that the combination of iKera cells and ECM resulted in the most desirable wound healing outcome, complete wound healing and re-epithelialization without excessive fibrosis. We also found that the conditioned medium of keratinocytes stimulated fibroblast proliferation, suggesting that the addition of keratinocytes may enhance fibroblast functions *in vivo*.

Building a skin tension model is essential for analyzing the impact of tension on skin wound healing. In our project, neither the experimental group nor the control group used the tension model, as the study's purpose was not to investigate the effects of tension on wounds. Furthermore, the healing effects of varying tension levels on skin defects differ significantly. Under tension-free conditions, the wound expands due to the contraction of the skin at the wound's edges, while moderate tension can stimulate cell proliferation and promote healing. However, excessive tension may lead to wound hardening, decreased skin elasticity, skin ischemia, and delayed healing. Therefore, there are stringent requirements regarding the magnitude of tension during the skin healing process. Some skin wound models that simulate tension utilize silicone gaskets; however, the tension cannot be adjusted during this process, and standardizing the tension size is challenging, as it is influenced by factors such as the size, thickness, number of sutures, suture tension force, and suture distance of the silicone gasket [86,87]. Consequently, not all skin defect models need to consider tension factors, especially in the absence of ideal animal models. Additionally, whether ECM alone or in combination with iKera cells is beneficial for wound healing in the presence of tension warrants further exploration in a more ideal tension-affected wound healing model.

Our findings demonstrate that dermal ECM scaffolds can create a favorable environment for keratinocytes and other important cells to achieve optimal cutaneous wound healing. Decellularized ECM has long been used as scaffolds for *in vivo* implantations of primary human cells, stem cells, and induced pluripotent stem cells in biomedical research and tissue engineering, as well as used wound dressing (such as OASIS by Smith + Nephew USA) [84,85,88]. While ECM is a complex structure composed of macromolecules, primarily containing type I and type III collagen, fibronectin, elastin, and various proteoglycans, although extensive proteomic studies have uncovered hundreds of proteins [89,90]. It is now well recognized that ECM not only maintains tissue dynamic integrity but also acts on numerous signaling pathways. Regardless of its source, ECM is usually decellularized through biological, chemical, or enzymatic methods while preserving the natural structure of the ECM, including components such as growth factors and cytokines in the matrix. While decellularized ECM can be isolated from virtually all types of organs and/or tissues, the ECM structures and/or compositions may vary significantly among ages, tissue types, and species [63,91,92]. Natural biomaterials similar to ECM, such as collagen, gelatin, and hyaluronic acid, have also been commonly used in wound repair and wound dressings although they may lack the molecular complexity and heterogeneity of the tissue-derived ECM [93].

More recently, cell-derived ECM has become an emerging field that offers a more convenient and customizable source of ECM production than decellularized tissues. For instance, drugs can be utilized to influence matrix deposition, or modifying the genotype of the source cells can manipulate the levels of growth factors in the ECM [94,95]. In our study, the decellularization process was easily accomplished by using DNase to effectively eliminate the nucleic acid components, thereby reducing the immunogenicity of the ECM. Our *in vivo* studies indicate that the decellularized ECM prepared from imDFs exhibited low immunogenicity and relatively rapid degradation *in vivo*. Thus, the reported imDFs may be used as a valuable cell source for generating a large quantity of dermal-specific ECM in skin tissue engineering.

5. Conclusions

Herein, we investigated the interactions between dermal fibroblasts or ECM-derived from dermal fibroblasts and keratinocytes on the scarless healing of cutaneous wounds. To overcome the limited lifespan of primary dermal fibroblasts, we established a reversibly immortalized mouse dermal fibroblasts (imDFs), which were non-tumorigenic, expressed dermal fibroblast markers and were responsive to TGF-β1 stimulation. The ECM prepared from both imDFs and primary dermal fibroblasts shared similar expression profiles of extracellular matrix proteins, and promoted the proliferation of keratinocytes iKera cells. The imDFs-ECM did not solicit local immune response. While the ECM and to a lesser extent imDFs promoted mouse skin wound healing with excessive fibrosis, a combination of imDFs-ECM and iKera effectively promoted the re-epithelization and scarless healing of skin wounds in a mouse model. These findings strongly suggest that dermal fibroblast-derived ECM, not fibroblasts themselves, may synergize with keratinocytes in controlling scarless healing and re-epithelialization of skin wounds. Given its low immunogenic nature, imDFs-ECM should be a valuable resource of skin-specific biomaterial for wound healing and skin regeneration.

CRediT authorship contribution statement

Xiangyu Dong: Writing – review & editing, Writing – original draft, Validation, Methodology, Investigation, Formal analysis, Data curation, Conceptualization. **Han Xiang:** Writing – review & editing, Writing – original draft, Validation, Methodology, Formal analysis, Data curation. **Jiajia Li:** Writing – review & editing, Writing – original draft, Validation, Methodology, Investigation, Formal analysis, Data curation, Conceptualization. **Ailing Hao:** Writing – review & editing, Validation, Resources, Methodology, Investigation, Formal analysis. **Hao Wang:** Writing – review & editing, Validation, Resources, Methodology, Investigation, Formal analysis. **Yannian Gou:** Writing – review & editing, Validation, Resources, Methodology, Investigation, Formal analysis. **Aohua Li:** Writing – review & editing, Validation, Resources, Methodology, Data curation. **Saidur Rahaman:** Writing – review & editing, Validation, Resources, Methodology, Formal analysis. **Yiheng Qiu:** Writing – review & editing, Validation, Resources, Methodology. **Jiahao Li:** Writing – review & editing, Validation, Resources, Methodology, Formal analysis. **Ou Mei:** Writing – review & editing, Validation, Resources, Methodology. **Jiamin Zhong:** Writing – review & editing, Validation, Resources, Methodology, Investigation, Formal analysis, Data curation. **Wulin You:** Writing – review & editing, Validation, Resources, Methodology, Investigation. **Guowei Shen:** Writing – review & editing, Validation, Resources, Methodology. **Xingye Wu:** Writing – review & editing, Validation, Resources, Methodology, Formal analysis.

Jingjing Li: Writing – review & editing, Validation, Resources, Methodology. **Yi Shu:** Writing – review & editing, Validation, Resources, Methodology, Investigation. **Lewis L. Shi:** Writing – review & editing, Writing – original draft, Supervision, Formal analysis, Conceptualization. **Yi Zhu:** Writing – review & editing, Writing – original draft, Validation, Resources, Methodology, Investigation, Formal analysis, Conceptualization. **Russell R. Reid:** Writing – review & editing, Writing – original draft, Supervision, Project administration, Investigation, Funding acquisition, Conceptualization. **Tong-Chuan He:** Writing – review & editing, Writing – original draft, Validation, Supervision, Project administration, Investigation, Funding acquisition, Formal analysis, Data curation, Conceptualization. **Jiaming Fan:** Writing – review & editing, Writing – original draft, Validation, Supervision, Methodology, Funding acquisition, Formal analysis, Data curation, Conceptualization.

Data and materials availability

All data are available in the main text or the supplementary materials.

Ethics approval and consent to participate

No human subjects and clinical samples were involved in the reported work. The use and care of experimental animals were approved by the Research Ethics and Regulatory Committee of Chongqing Medical University, China, and the Institutional Animal Care and Use Committee of The University of Chicago, in compliance with all relevant ethical regulations.

Declaration of competing interest

The authors declare no competing interests.

Acknowledgements

The reported study was supported in part by research grants from the Natural Science Foundation of China (82102696, JF), Chongqing Natural Science Foundation (2024NSCQ-MSX0073, JF), and the National Institutes of Health (CA226303 to TCH, and DE030480 to RRR). This project was also supported in part by The University of Chicago Comprehensive Cancer Center Support Grant (P30CA014599) and the National Center for Advancing Translational Sciences of the National Institutes of Health through Grant Number UL1 TR000430. TCH was supported by the Mabel Green Myers Research Endowment Fund and The University of Chicago Orthopaedics Alumni Fund. Funding sources were not involved in the study design; in the collection, analysis and interpretation of data; in the writing of the report; and in the decision to submit the paper for publication.

Appendix A. Supplementary data

Supplementary data to this article can be found online at https://doi.org/10.1016/j.bioactmat.2024.12.030.

References

[1] I.A. Darby, B. Laverdet, F. Bonté, A. Desmoulière, Fibroblasts and myofibroblasts in wound healing, Clin. Cosmet. Invest. Dermatol. 7 (2014) 301–311, https://doi.org/10.2147/ccid.S50046.
[2] M. Rodrigues, N. Kosaric, C.A. Bonham, G.C. Gurtner, Wound healing: a cellular perspective, Physiol. Rev. 99 (2019) 665–706, https://doi.org/10.1152/physrev.00067.2017.
[3] G.C. Gurtner, S. Werner, Y. Barrandon, M.T. Longaker, Wound repair and regeneration, Nature 453 (2008) 314–321, https://doi.org/10.1038/nature07039.
[4] T. Bensa, S. Tekkela, E. Rognoni, Skin fibroblast functional heterogeneity in health and disease, J. Pathol. 260 (2023) 609–620, https://doi.org/10.1002/path.6159.
[5] S. Abbasi, et al., Distinct regulatory programs control the latent regenerative potential of dermal fibroblasts during wound healing, Cell Stem Cell 27 (2020) 396–412.e396, https://doi.org/10.1016/j.stem.2020.07.008.
[6] V. Thulabandu, D. Chen, R.P. Atit, Dermal fibroblast in cutaneous development and healing, Wiley Interdiscip Rev Dev Biol 7 (2018), https://doi.org/10.1002/wdev.307.
[7] M. Xue, R. Zhao, L. March, C. Jackson, Dermal fibroblast heterogeneity and its contribution to the skin repair and regeneration, Adv. Wound Care 11 (2022) 87–107, https://doi.org/10.1089/wound.2020.1287.
[8] H.E. Talbott, S. Mascharak, M. Griffin, D.C. Wan, M.T. Longaker, Wound healing, fibroblast heterogeneity, and fibrosis, Cell Stem Cell 29 (2022) 1161–1180, https://doi.org/10.1016/j.stem.2022.07.006.
[9] J. Li, Y. Chen, M. Tiwari, V. Bansal, G.L. Sen, Regulation of integrin and extracellular matrix genes by HNRNPL is necessary for epidermal renewal, PLoS Biol. 19 (2021) e3001378, https://doi.org/10.1371/journal.pbio.3001378.
[10] R.O. Hynes, The extracellular matrix: not just pretty fibrils, Science (New York, N. Y.) 326 (2009) 1216–1219, https://doi.org/10.1126/science.1176009.
[11] M. Mohammadi, S.K. Olsen, R. Goetz, A protein canyon in the FGF-FGF receptor dimer selects from an à la carte menu of heparan sulfate motifs, Curr. Opin. Struct. Biol. 15 (2005) 506–516, https://doi.org/10.1016/j.sbi.2005.09.002.
[12] M.F. Brizzi, G. Tarone, P. Defilippi, Extracellular matrix, integrins, and growth factors as tailors of the stem cell niche, Curr. Opin. Cell Biol. 24 (2012) 645–651, https://doi.org/10.1016/j.ceb.2012.07.001.
[13] Y. Song, et al., Adipose-derived mesenchymal stem cell-derived exosomes biopotentiated extracellular matrix hydrogels accelerate diabetic wound healing and skin regeneration, Adv. Sci. 10 (2023) e2304023, https://doi.org/10.1002/advs.202304023.
[14] W. Liu, et al., ECM-mimetic immunomodulatory hydrogel for methicillin-resistant Staphylococcus aureus-infected chronic skin wound healing, Sci. Adv. 8 (2022) eabn7006, https://doi.org/10.1126/sciadv.abn7006.
[15] F. Santarella, et al., Scaffolds functionalized with matrix from induced pluripotent stem cell fibroblasts for diabetic wound healing, Adv. Healthcare Mater. 9 (2020) e2000307, https://doi.org/10.1002/adhm.202000307.
[16] P. Du, et al., Human lung fibroblast-derived matrix facilitates vascular morphogenesis in 3D environment and enhances skin wound healing, Acta Biomater. 54 (2017) 333–344, https://doi.org/10.1016/j.actbio.2017.03.035.
[17] M. Jevtic, et al., Impact of intercellular crosstalk between epidermal keratinocytes and dermal fibroblasts on skin homeostasis, Biochim. Biophys. Acta Mol. Cell Res. 1867 (2020) 118722, https://doi.org/10.1016/j.bbamcr.2020.118722.
[18] N. Amiri, A.P. Golin, R.B. Jalili, A. Ghahary, Roles of cutaneous cell-cell communication in wound healing outcome: an emphasis on keratinocyte-fibroblast crosstalk, Exp. Dermatol. 31 (2022) 475–484, https://doi.org/10.1111/exd.14516.
[19] J. Zhong, et al., Reversibly immortalized keratinocytes (iKera) facilitate re-epithelization and skin wound healing: potential applications in cell-based skin tissue engineering, Bioact. Mater. 9 (2022) 523–540, https://doi.org/10.1016/j.bioactmat.2021.07.022.
[20] Q. Wei, et al., Engineering the rapid adenovirus production and amplification (RAPA) cell line to expedite the generation of recombinant adenoviruses, Cell. Physiol. Biochem. : Intern. J. Expe. cell. Physio. Biochem. Pharmaco. 41 (2017) 2383–2398, https://doi.org/10.1159/000475909.
[21] N. Wu, et al., Overexpression of Ad5 precursor terminal protein accelerates recombinant adenovirus packaging and amplification in HEK-293 packaging cells, Gene Ther. 21 (2014) 629–637, https://doi.org/10.1038/gt.2014.40.
[22] G. Zhao, et al., GAPDH suppresses adenovirus-induced oxidative stress and enables a superfast production of recombinant adenovirus, Genes Dis. 11 (2024) 101344, https://doi.org/10.1016/j.gendis.2024.101344.
[23] X. Dong, et al., A simplified noncryogenic strategy to transport mesenchymal stem cells: potential applications in cell therapy and regenerative medicine, Genes Dis. 11 (2024) 101073, https://doi.org/10.1016/j.gendis.2023.07.002.
[24] J. Liu, et al., A single dose of VEGF-A circular RNA sustains in situ long-term expression of protein to accelerate diabetic wound healing, J. Contr. Release : Offic. J. Contro. Rele. Soc. 373 (2024) 319–335, https://doi.org/10.1016/j.jconrel.2024.07.018.
[25] E. Huang, et al., Conditionally immortalized mouse embryonic fibroblasts retain proliferative activity without compromising multipotent differentiation potential, PLoS One 7 (2012) e32428, https://doi.org/10.1371/journal.pone.0032428.
[26] Y. Gou, et al., Adipose-derived mesenchymal stem cells (MSCs) are a superior cell source for bone tissue engineering, Bioact. Mater. 34 (2024) 51–63, https://doi.org/10.1016/j.bioactmat.2023.12.003.
[27] Y. Bi, et al., Functional characteristics of reversibly immortalized hepatic progenitor cells derived from mouse embryonic liver, Cell. Physiol. Biochem. : Intern. J. Expe. cell. Physio. Biochem. Pharmaco. 34 (2014) 1318–1338, https://doi.org/10.1159/000366340.
[28] M. Li, et al., Establishment and characterization of the reversibly immortalized mouse fetal heart progenitors, Int. J. Med. Sci. 10 (2013) 1035–1046, https://doi.org/10.7150/ijms.6639.
[29] N. Wang, et al., The piggyBac transposon-mediated expression of SV40 T antigen efficiently immortalizes mouse embryonic fibroblasts (MEFs), PLoS One 9 (2014) e97316, https://doi.org/10.1371/journal.pone.0097316.
[30] J. Luo, et al., A protocol for rapid generation of recombinant adenoviruses using the AdEasy system, Nat. Protoc. 2 (2007) 1236–1247, https://doi.org/10.1038/nprot.2007.135.
[31] Y. Gou, et al., Carboxymethyl chitosan prolongs adenovirus-mediated expression of IL-10 and ameliorates hepatic fibrosis in a mouse model, Bioeng Transl. Med. 7 (2022) e10306, https://doi.org/10.1002/btm2.10306.

[32] C.S. Lee, et al., Adenovirus-mediated gene delivery: potential applications for gene and cell-based therapies in the new era of personalized medicine, Genes Dis. 4 (2017) 43–63, https://doi.org/10.1016/j.gendis.2017.04.001.
[33] S.K. Denduluri, et al., Immortalized mouse achilles tenocytes demonstrate long-term proliferative capacity while retaining tenogenic properties, Tissue Eng. C Methods 22 (2016) 280–289, https://doi.org/10.1089/ten.tec.2015.0244.
[34] Y. Yu, et al., SV40 large T antigen-induced immortalization reprograms mouse cardiomyocyte progenitors with mesenchymal stem cell characteristics and osteogenic potential, Genes Dis. 10 (2023) 1161–1164, https://doi.org/10.1016/j.gendis.2022.10.008.
[35] C. Zhao, et al., Adenovirus-mediated gene transfer in mesenchymal stem cells can be significantly enhanced by the cationic polymer polybrene, PLoS One 9 (2014) e92908, https://doi.org/10.1371/journal.pone.0092908.
[36] J. Liao, et al., lncRNA H19 mediates BMP9-induced osteogenic differentiation of mesenchymal stem cells (MSCs) through Notch signaling, Oncotarget 8 (2017) 53581–53601, https://doi.org/10.18632/oncotarget.18655.
[37] M.R. Rogers, et al., Bone Morphogenic Protein 9 (BMP9)/Growth Differentiation Factor 2 (GDF2) modulates mouse adult hippocampal neurogenesis by regulating the survival of early neural progenitors, Genes Dis. 10 (2023) 1175–1179, https://doi.org/10.1016/j.gendis.2023.02.018.
[38] L. Huang, et al., Niclosamide (NA) overcomes cisplatin resistance in human ovarian cancer, Genes Dis. 10 (2023) 1687–1701, https://doi.org/10.1016/j.gendis.2022.12.005.
[39] F. He, et al., OUHP: an optimized universal hairpin primer system for cost-effective and high-throughput RT-qPCR-based quantification of microRNA (miRNA) expression, Nucleic Acids Res. 50 (2022) e22, https://doi.org/10.1093/nar/gkab1153.
[40] Q. Zhang, et al., TqPCR: a touchdown qPCR assay with significantly improved detection sensitivity and amplification efficiency of SYBR green qPCR, PLoS One 10 (2015) e0132666, https://doi.org/10.1371/journal.pone.0132666.
[41] Y. Deng, et al., A blockade of IGF signaling sensitizes human ovarian cancer cells to the anthelmintic niclosamide-induced anti-proliferative and anticancer activities, Cell. Physiol. Biochem. : Intern. J. Expe. cell. Physio. Biochem. Pharmaco. 39 (2016) 871–888, https://doi.org/10.1159/000447797.
[42] Y. Deng, et al., Antibiotic monensin synergizes with EGFR inhibitors and oxaliplatin to suppress the proliferation of human ovarian cancer cells, Sci. Rep. 5 (2015) 17523, https://doi.org/10.1038/srep17523.
[43] R. Li, et al., Targeting BMP9-promoted human osteosarcoma growth by inactivation of notch signaling, Curr. Cancer Drug Targets 14 (2014) 274–285.
[44] X. Wang, et al., Decellularized liver scaffolds effectively support the proliferation and differentiation of mouse fetal hepatic progenitors, J. Biomed. Mater. Res. 102 (2014) 1017–1025, https://doi.org/10.1002/jbm.a.34764.
[45] M. Ghetti, et al., Subpopulations of dermal skin fibroblasts secrete distinct extracellular matrix: implications for using skin substitutes in the clinic, Br. J. Dermatol. 179 (2018) 381–393, https://doi.org/10.1111/bjd.16255.
[46] S. Nellinger, et al., Cell-derived and enzyme-based decellularized extracellular matrix exhibit compositional and structural differences that are relevant for its use as a biomaterial, Biotechnol. Bioeng. 119 (2022) 1142–1156, https://doi.org/10.1002/bit.28047.
[47] F. Wang, et al., Fabrication of the FGF1-functionalized sericin hydrogels with cell proliferation activity for biomedical application using genetically engineered Bombyx mori (B. mori) silk, Acta Biomater. 79 (2018) 239–252, https://doi.org/10.1016/j.actbio.2018.08.031.
[48] X. Wang, et al., Monensin inhibits cell proliferation and tumor growth of chemo-resistant pancreatic cancer cells by targeting the EGFR signaling pathway, Sci. Rep. 8 (2018) 17914, https://doi.org/10.1038/s41598-018-36214-5.
[49] M. Duan, et al., Epidermal stem cell-derived exosomes promote skin regeneration by downregulating transforming growth factor-β1 in wound healing, Stem Cell Res. Ther. 11 (2020) 452, https://doi.org/10.1186/s13287-020-01971-6.
[50] L. An, et al., Bone morphogenetic protein 4 (BMP4) promotes hepatic glycogen accumulation and reduces glucose level in hepatocytes through mTORC2 signaling pathway, Genes Dis. 8 (2021) 531–544, https://doi.org/10.1016/j.gendis.2020.11.004.
[51] K. Yang, et al., Conditional immortalization establishes a repertoire of mouse melanocyte progenitors with distinct melanogenic differentiation potential, J. Invest. Dermatol. 132 (2012) 2479–2483, https://doi.org/10.1038/jid.2012.145.
[52] J.D. Lamplot, et al., Reversibly immortalized mouse articular chondrocytes acquire long-term proliferative capability while retaining chondrogenic phenotype, Cell Transplant. 24 (2015) 1053–1066, https://doi.org/10.3727/096368914X681054.
[53] S. Lu, et al., Bone morphogenetic protein 9 (BMP9) induces effective bone formation from reversibly immortalized multipotent adipose-derived (iMAD) mesenchymal stem cells, Am. J. Transl. Res. 8 (2016) 3710–3730.
[54] J. Wang, et al., Bone morphogenetic protein-9 effectively induces osteo/odontoblastic differentiation of the reversibly immortalized stem cells of dental apical papilla, Stem Cell. Dev. 23 (2014) 1405–1416, https://doi.org/10.1089/scd.2013.0580.
[55] M.D. Lynch, F.M. Watt, Fibroblast heterogeneity: implications for human disease, J. Clin. Invest. 128 (2018) 26–35, https://doi.org/10.1172/jci93555.
[56] M.F.P. Graça, S.P. Miguel, C.S.D. Cabral, I.J. Correia, Hyaluronic acid—based wound dressings: a review, Carbohydr. Polym. 241 (2020) 116364, https://doi.org/10.1016/j.carbpol.2020.116364.
[57] C. Dees, D. Chakraborty, J.H.W. Distler, Cellular and molecular mechanisms in fibrosis, Exp. Dermatol. 30 (2021) 121–131, https://doi.org/10.1111/exd.14193.
[58] T. Zhang, et al., Current potential therapeutic strategies targeting the TGF-β/Smad signaling pathway to attenuate keloid and hypertrophic scar formation, Biomed. pharmacoth. 129 (2020) 110287, https://doi.org/10.1016/j.biopha.2020.110287.
[59] R.B. Diller, A.J. Tabor, The role of the extracellular matrix (ECM) in wound healing: a review, Biomimetics 7 (2022), https://doi.org/10.3390/biomimetics7030087.
[60] A.D. Theocharis, S.S. Skandalis, C. Gialeli, N.K. Karamanos, Extracellular matrix structure, Adv. Drug Deliv. Rev. 97 (2016) 4–27, https://doi.org/10.1016/j.addr.2015.11.001.
[61] A. Nyström, L. Bruckner-Tuderman, Matrix molecules and skin biology, Semin. Cell Dev. Biol. 89 (2019) 136–146, https://doi.org/10.1016/j.semcdb.2018.07.025.
[62] J. Huang, et al., Dermal extracellular matrix molecules in skin development, homeostasis, wound regeneration and diseases, Semin. Cell Dev. Biol. 128 (2022) 137–144, https://doi.org/10.1016/j.semcdb.2022.02.027.
[63] J.M. Aamodt, D.W. Grainger, Extracellular matrix-based biomaterial scaffolds and the host response, Biomaterials 86 (2016) 68–82, https://doi.org/10.1016/j.biomaterials.2016.02.003.
[64] Y.K. Alshoubaki, et al., A superior extracellular matrix binding motif to enhance the regenerative activity and safety of therapeutic proteins, NPJ Regenerative Med. 8 (2023) 25, https://doi.org/10.1038/s41536-023-00297-0.
[65] R. Lang, D. Patel, J.J. Morris, R.L. Rutschman, P.J. Murray, Shaping gene expression in activated and resting primary macrophages by IL-10, J. immunol. (169) (1950) 2253–2263, https://doi.org/10.4049/jimmunol.169.5.2253, 2002.
[66] A. Shapouri-Moghaddam, et al., Macrophage plasticity, polarization, and function in health and disease, J. Cell. Physiol. 233 (2018) 6425–6440, https://doi.org/10.1002/jcp.26429.
[67] X. Xia, et al., Neutrophil extracellular traps promote metastasis in gastric cancer patients with postoperative abdominal infectious complications, Nat. Commun. 13 (2022) 1017, https://doi.org/10.1038/s41467-022-28492-5.
[68] J. Mo, et al., Humanized neurofibroma model from induced pluripotent stem cells delineates tumor pathogenesis and developmental origins, J. Clin. Invest. 131 (2021), https://doi.org/10.1172/jci139807.
[69] X. Zhang, et al., Combination cancer immunotherapy targeting TNFR2 and PD-1/PD-L1 signaling reduces immunosuppressive effects in the microenvironment of pancreatic tumors, J. immunothe. cancer 10 (2022), https://doi.org/10.1136/jitc-2021-003982.
[70] X. Liu, et al., RNAi functionalized collagen-chitosan/silicone membrane bilayer dermal equivalent for full-thickness skin regeneration with inhibited scarring, Biomaterials 34 (2013) 2038–2048, https://doi.org/10.1016/j.biomaterials.2012.11.062.
[71] Y. Dong, et al., Conformable hyaluronic acid hydrogel delivers adipose-derived stem cells and promotes regeneration of burn injury, Acta Biomater. 108 (2020) 56–66, https://doi.org/10.1016/j.actbio.2020.03.040.
[72] E.N. Lamme, R.T. Van Leeuwen, K. Brandsma, J. Van Marle, E. Middelkoop, Higher numbers of autologous fibroblasts in an artificial dermal substitute improve tissue regeneration and modulate scar tissue formation, J. Pathol. 190 (2000) 595–603, https://doi.org/10.1002/(sici)1096-9896(200004)190:5<595::Aid-path572>3.0.Co;2-v.
[73] K. Ueno, et al., Treatment of refractory cutaneous ulcers with mixed sheets consisting of peripheral blood mononuclear cells and fibroblasts, Sci. Rep. 6 (2016) 28538, https://doi.org/10.1038/srep28538.
[74] W. Xiaojie, et al., Scarless wound healing: current insights from the perspectives of TGF-β, KGF-1, and KGF-2, Cytokine Growth Factor Rev. 66 (2022) 26–37, https://doi.org/10.1016/j.cytogfr.2022.03.001.
[75] C. Ruiz-Cañada, Á. Bernabé-García, S. Liarte, M. Rodríguez-Valiente, F.J. Nicolás, Chronic wound healing by amniotic membrane: TGF-β and EGF signaling modulation in Re-epithelialization, Front. Bioeng. Biotechnol. 9 (2021) 689328, https://doi.org/10.3389/fbioe.2021.689328.
[76] I.C. Le Poole, S.T. Boyce, Keratinocytes suppress transforming growth factor-beta1 expression by fibroblasts in cultured skin substitutes, Br. J. Dermatol. 140 (1999) 409–416, https://doi.org/10.1046/j.1365-2133.1999.02700.x.
[77] F. De Francesco, A. Saparov, M. Riccio, Hyaluronic acid accelerates re-epithelialization and healing of acute cutaneous wounds, Eur. Rev. Med. Pharmacol. Sci. 27 (2023) 37–45, https://doi.org/10.26355/eurrev_202304_31320.
[78] A. Stunova, L. Vistejnova, Dermal fibroblasts-A heterogeneous population with regulatory function in wound healing, Cytokine Growth Factor Rev. 39 (2018) 137–150, https://doi.org/10.1016/j.cytogfr.2018.01.003.
[79] D.A.C. Walma, K.M. Yamada, The extracellular matrix in development, Development 147 (2020), https://doi.org/10.1242/dev.175596.
[80] S. Chakravarti, E. Enzo, M. Rocha Monteiro de Barros, M.B.R. Maffezzoni, G. Pellegrini, Genetic disorders of the extracellular matrix: from cell and gene therapy to future applications in regenerative medicine, Annu. Rev. Genom. Hum. Genet. 23 (2022) 193–222, https://doi.org/10.1146/annurev-genom-083117-021702.
[81] N.N. Potekaev, et al., The role of extracellular matrix in skin wound healing, J. Clin. Med. 10 (2021), https://doi.org/10.3390/jcm10245947.
[82] M. Xue, C.J. Jackson, Extracellular matrix reorganization during wound healing and its impact on abnormal scarring, Adv. Wound Care 4 (2015) 119–136, https://doi.org/10.1089/wound.2013.0485.
[83] J. Li, et al., Spatially resolved proteomic map shows that extracellular matrix regulates epidermal growth, Nat. Commun. 13 (2022) 4012, https://doi.org/10.1038/s41467-022-31659-9.
[84] H. Capella-Monsonis, R.J. Crum, G.S. Hussey, S.F. Badylak, Advances, challenges, and future directions in the clinical translation of ECM biomaterials for

regenerative medicine applications, Adv. Drug Deliv. Rev. 211 (2024) 115347, https://doi.org/10.1016/j.addr.2024.115347.
[85] A. Smandri, M.E. Al-Masawa, N.M. Hwei, M.B. Fauzi, ECM-derived biomaterials for regulating tissue multicellularity and maturation, iScience 27 (2024) 109141, https://doi.org/10.1016/j.isci.2024.109141.
[86] B. Hinz, D. Mastrangelo, C.E. Iselin, C. Chaponnier, G. Gabbiani, Mechanical tension controls granulation tissue contractile activity and myofibroblast differentiation, Am. J. Pathol. 159 (2001) 1009–1020, https://doi.org/10.1016/s0002-9440(10)61776-2.
[87] Y. Yang, et al., Splint-free line drawing model: an innovative method for excisional wound models, Int. Wound J. 20 (2023) 2673–2678, https://doi.org/10.1111/iwj.14141.
[88] H. Xing, H. Lee, L. Luo, T.R. Kyriakides, Extracellular matrix-derived biomaterials in engineering cell function, Biotechnol. Adv. 42 (2020) 107421, https://doi.org/10.1016/j.biotechadv.2019.107421.
[89] T.E. Sutherland, D.P. Dyer, J.E. Allen, The extracellular matrix and the immune system: a mutually dependent relationship, Science (New York, N.Y.) 379 (2023) eabp8964, https://doi.org/10.1126/science.abp8964.
[90] A. Naba, Ten years of extracellular matrix proteomics: accomplishments, challenges, and future perspectives, Mol. Cell. Proteomics 22 (2023) 100528, https://doi.org/10.1016/j.mcpro.2023.100528.
[91] R.M. Wang, et al., Humanized mouse model for assessing the human immune response to xenogeneic and allogeneic decellularized biomaterials, Biomaterials 129 (2017) 98–110, https://doi.org/10.1016/j.biomaterials.2017.03.016.
[92] S. Tottey, et al., The effect of source animal age upon extracellular matrix scaffold properties, Biomaterials 32 (2011) 128–136, https://doi.org/10.1016/j.biomaterials.2010.09.006.
[93] C. Savitri, S.S. Ha, E. Liao, P. Du, K. Park, Extracellular matrices derived from different cell sources and their effect on macrophage behavior and wound healing, J. Mater. Chem. B 8 (2020) 9744–9755, https://doi.org/10.1039/d0tb01885f.
[94] S. Han, Y.Y. Li, B.P. Chan, Protease inhibitors enhance extracellular collagen fibril deposition in human mesenchymal stem cells, Stem Cell Res. Ther. 6 (2015) 197, https://doi.org/10.1186/s13287-015-0191-1.
[95] S. Zeitouni, et al., Human mesenchymal stem cell-derived matrices for enhanced osteoregeneration, Sci. Transl. Med. 4 (2012) 132ra155, https://doi.org/10.1126/scitranslmed.3003396.